Journal of Sedimentary Research

Journal of Sedimentary Research, 2013, v. 83, 1162–1180
Research Article
DOI: 10.2110/jsr.2013.91

EXPERIMENTAL INVESTIGATION OF SEDIMENT-DOMINATED VS. TECTONICS-DOMINATED SEDIMENT TRANSPORT SYSTEMS IN SUBSIDING BASINS

KYLE M. STRAUB,[1] CHRIS PAOLA,[2] WONSUCK KIM,[3] AND BEN SHEETS[4]
[1] *Department of Earth and Environmental Sciences, Tulane University, New Orleans, Louisiana 70118, U.S.A.*
[2] *Department of Earth Sciences, St. Anthony Falls Laboratory, University of Minnesota, Minneapolis, Minnesota 55414, U.S.A.*
[3] *Department of Geological Sciences, University of Texas at Austin, Austin, Texas 78712, U.S.A.*
[4] *Barr Engineering Company, Minneapolis, Minnesota 55435, U.S.A.*
e-mail: kmstraub@tulane.edu

ABSTRACT: **Models of stratigraphic architecture make testable predictions regarding the subsurface spatial density and connectivity of channel sandstone bodies in subsiding basins. Here we test one of these predictions: that lateral gradients of subsidence rate in alluvial basins tend to draw channels to local subsidence maxima and thus increase the subsurface stacking density of channel sand bodies in the vicinity of subsidence maxima. Here we define channel steering as any change in channel course due to lateral gradients in subsidence, focusing on the attraction of channels to regions of high subsidence. We examine the hypothesis that steering is controlled by the *tilting ratio*: the ratio of the rate of lateral tilting to that of lateral channel mobility, with steering effects expected to increase as the tilting ratio increases. We present measurements of channel steering from experiments in which we varied the tilting ratio over four stages. The experiments used a relay-ramp geometry with laterally variable uplift and subsidence. Initially, with a small value of the tilting ratio, we did not detect noticeable channel steering. Through reductions in input sediment discharge (Q_s) and water discharge (Q_w) we decreased channel mobility in later stages while keeping the subsidence regime the same. This resulted in systematic increases in the tilting ratio and in observable steering towards regions of high subsidence. Interestingly, the increase in tilting rate relative to channel mobility also resulted in a preference for channel occupation over uplift regions as channels were trapped by incision into the rising surface. We also develop theory to predict when the strength and duration of pulsed tilting events are sufficient to steer channels. As with the theory for steady subsidence, the new theory suggests that pulsed events must be strong enough and long-lived enough to produce comparable cross-basin to down-basin transport slopes. An experimental stage with pulsed tectonics supports this theory. Finally, we document autogenic shoreline transgressions in the relay zone during deformation. These transgressions produce downstream to upstream facies translation of the sand–coal boundary in the preserved stratigraphy and illustrate a mechanism by which transgressions can develop without external cause.**

INTRODUCTION

Roughly thirty-five years ago a series of papers by Leeder (1978), Allen (1978), and Bridge and Leeder (1979) and later extended by Alexander and Leeder (1987) presented the first suite of quantitative alluvial-architecture models. These studies focused on the relationship between subsidence rate and the subsurface spatial density and connectivity of channel sandstone bodies. These models have strongly influenced the fields of basin analysis and stratigraphy; they offer clear, testable predictions about the architecture of stratigraphy in subsiding basins that have important consequences for both basic and applied research. In this paper, we focus on just one of these predictions, that lateral gradients of subsidence rate in alluvial basins tend to draw channels to local subsidence maxima and thus increase the subsurface stacking density of channel sand bodies going towards the subsidence maxima (Alexandar and Leeder 1987). Further work on the role of lateral ground tilting on sediment routing systems is motivated by the desire to improve prediction of subsurface reservoirs and reconstruction of basin evolution from preserved stratigraphy (Marzo et al. 1988; Mack and Seager 1990; Melvin 1993; Ryseth and Ramm 1996; Gouw 2008).

Since publication of the model of Alexander and Leeder (1987), several researchers have examined the influence of lateral subsidence gradient on the geomorphology and stratigraphy of sediment routing systems through field campaigns (Alexander and Leeder 1990; Maccarthy 1990; Kraus 1992; Leeder et al. 1996; Peakall 1998; Peakall et al. 2000) and physical experiments (Ouchi 1985; Schumm et al. 1987; Cazanacli et al. 2002; Hickson et al. 2005; Kim and Paola 2007; Kim et al. 2010). Several field studies noted high channel stacking in basin stratigraphy near extensional faults (Alexander and Leeder 1990; Maccarthy 1990; Kraus 1992). A later extensive field study of the Rio Grande Rift reported by Leeder et al. (1996) and Peakall (1998), while generally supporting Alexander and Leeder's hypothesis, does not include the complete coupling of surface evolution to resulting stratigraphy in three dimensions. Unfortunately, to date these two studies of the Rio Grande Rift system are the only quantitative test of the influence of lateral ground tilting on steering of channels with field data. Constraining model parameters from field observations has proved difficult.

Some of the physical experiments designed to examine the influence of lateral subsidence gradients on sediment transport systems have indicated

Published Online: January 2014
 1527-1404/13/083-1162/$03.00

that lateral basin tilting can steer channels (Ouchi 1985; Schumm et al. 1987; Kim and Paola 2007; Kim et al. 2010) while others have not (Cazanacli et al. 2002; Hickson et al. 2005). Here we focus on a suite of experiments preformed in the Experimental EarthScape (XES) basin at the St. Anthony Falls Laboratory (SAFL). The XES basin allows study of geomorphic processes and their resulting stratigraphy in a basin with independently controlled water and sediment supplies, base level, and rate and geometry of subsidence (Paola 2000; Heller et al. 2001; Paola et al. 2001; Sheets et al. 2002; Strong et al. 2005; Kim et al. 2011). The basin is 5.82 m long and 2.98 m wide, and is underlain by 108 independently controlled subsiding cells. Gradual removal of well-sorted, pea-size gravel from the base of each subsiding cell allows generation of a range of spatial and temporal subsidence patterns.

The first experiment in the XES basin to investigate steering of channels due to lateral basin tilting and the stacking of channelized deposits, XES 99, was performed in 1999 and is analyzed in Cazanacli et al. (2002), Sheets et al. (2002), Strong et al. (2005), and Hickson et al. (2005). The XES 99 experiment began with two stages designed to investigate the effect of lateral basin tilting on channel stacking. With the exception of overall subsidence rate and geometry, all additional experimental parameters were kept constant in the two stages. Further, input sediment discharge matched the generation of accommodation upstream of the shoreline in each stage of the experiment, resulting in an approximately stable shoreline location throughout both stages. The first stage had asymmetric cross-stream subsidence, with maximum subsidence located roughly one third of the way across the basin. In the second stage of XES 99 the subsidence increased linearly down system with no lateral variability. While subsidence rate and geometry varied between the two stages, within each stage subsidence rate was steady in time. Application of Alexander and Leeder's (1987) theory would predict steering of channels in the first stage of the experiment towards the cross-stream subsidence maximum, and an associated maximum in preserved channel-bodies at this location in the preserved stratigraphy. No channel steering or cross-stream changes in stratigraphy would be predicted for the second stage. However, the analysis performed by Hickson et al. (2005) showed no apparent increase in channel body density over the cross-stream subsidence maximum. Using images of the preserved stratigraphy from eight strike-oriented cross sections, Hickson et al. mapped the locations of preserved channel bodies and used this information to quantify channel-body density. Further, in an analysis of overhead images of the experimental surface, Hickson et al. did not detect a preference for channel location over the subsidence maximum or a preference for rotation of flow (i.e., steering) into the subsidence maximum.

In an effort to explain the apparent contradiction of results in the XES 99 experiment with the theory of Alexander and Leeder (1987), Hickson et al. (2005) compared two time scales important to channel steering. These two time scales characterize the mobility of channels in relation to the width of a subsiding basin, versus the time necessary to develop a cross-stream slope, through differential subsidence, comparable to the slope in the dominant long-term flow direction. We term this non-dimensional ratio the "tilting ratio." As reported by Hickson et al., the high sediment-to-water ratio and noncohesive sediment used in XES 99, coupled with the modest cross-stream subsidence rate gradient in the experiment, resulted in a mobile transport system that was able to rework the surface topography to grade before a significant cross-stream slope could develop. It is worth noting that this result is not at odds with the theory of Alexander and Leeder (1987). In their work, Alexander and Leeder note that high aggradation rates could shift channel-belt deposition away from subsidence maxima and that the distribution of channel fills could prove problematic in determining the location of zones of differential subsidence. This observation was also made in a later numerical study by Mackey and Bridge (1995).

Motivated by the theory presented by Hickson et al. (2005), Kim and Paola (2007) and Kim et al. (2010) designed and conducted an experiment in the XES basin in 2005. This experiment, referred to as XES 05, was designed with a subsidence pattern meant to mimic a relay ramp in an extensional basin with *en echelon* fault geometry. The subsidence pattern in the relay zone was characterized by a strong cross-stream gradient in subsidence. Before the start of the experiment, several stages were designed with varying ratios of channel time scale to tectonic time scale. The experimental plan called for a first stage dominated by tectonics that would result in channel steering, followed by stages designed to have weaker steering, i.e., to be more "channel dominated." As in the XES 99 experiment, subsidence in the first stage of this experiment was steady in time. As reported in Kim and Paola (2007) and Kim et al. (2010) the first stage of the XES 05 experiment was successful in steering channels towards the subsidence maximum. Unfortunately, early in the second stage of XES 05 a failure of the subsidence mechanism near the inboard (upstream) fault of the relay ramp ended the experiment. As such, while XES 05 demonstrated that, given sufficiently fast tectonics and slow channel mobility, channels can be steered towards a subsidence maximum, the nature of the transition from channel-dominated to tectonics-dominated systems was unresolved. For example, given a constant tectonic environment, if channel mobility slowly decreased with time, would a system slowly convert from tectonics-dominated to channel-dominated, or would this transition occur abruptly due to a process threshold? And if there is a transition in behavior, how does steering change during the transition?

A second outstanding question involves temporal variation in tectonics. As discussed in Kim et al. (2010), all experiments performed in the XES basin to investigate the impact of lateral basin motion had temporally constant subsidence rates within any individual stage. However, subsidence can be highly unsteady in time (Wells and Coppersmith 1994). For example, many basins subside primarily via short-term, pulsed, or co-seismic slip along faults, while other basins accumulate accommodation through steady subsidence. At present, it remains unclear whether two basins, one coseismic the other aseismic, with the same long-term ratio of channel and tectonic time scales, are steered equally and if their stratigraphy would be similar. As discussed in Kim and Paola (2007) as well as in Ellis et al. (1999) and Allen and Densmore (2000), surface processes might help "smear" the transfer of tectonic signals into the stratigraphic record. Further, it is possible that long response times of transport systems to changes in tectonics might decrease the importance of unsteadiness in tectonics for the ability to steer channels (Allen and Densmore 2000).

In this paper, we report the results of the first experiment in which the time-scale ratio was systematically varied, with the same subsidence pattern, from conditions we expect to range from channel-dominated to tectonics-dominated. We focus on three questions. 1) Given a constant tectonic environment, but a range of channel mobilities, does the time-scale ratio correctly predict the change from channel-dominated to tectonics-dominated? 2) Is the change from one to the other gradual or associated with a process threshold? and 3) Is there a difference in surface processes and resulting stratigraphic architecture in pulsed versus steady basins with lateral subsidence gradients?

TECTONIC AND CHANNEL TIME SCALES

In this section we present theory that we use as a framework for defining the tilting ratio and thus differentiating channel-dominated versus tectonics-dominated systems. This theory is built upon the hypothesis that Hickson et al. (2005) posed to explain the lack of channel steering observed in the XES 99 experiment: that steering of channels by tectonics occurs only if the lateral gradient in subsidence rate is sufficiently high relative to the speed at which channels migrate over a

basin to allow the development of a cross-system slope comparable to the down-system slope. Kim et al. (2010) translated this hypothesis into a set of equations that define time scales associated with the mobility of channels (channel time scale, T_c) and the strength of tectonics (tectonic time scale, T_t). For convenience, we summarize this theory below.

In order for channels to be steered by tectonic tilting, thus exhibiting tectonic dominance, the tilting must be able to alter the path of steepest descent. This requires that

$$S_y \gtrsim S_x \tag{1}$$

where S_x is the sediment-surface slope in the dominant downstream direction and S_y is the slope in the cross-stream direction. This prediction distills the importance of tectonics with regards to channel steering to its ability to modify surface slopes relative to those produced by surface processes alone. Kim et al. (2010) emphasize that the relationship is not exact because of natural variability in topography induced by surface processes, including channel scour points and channel margins that work to direct flow over relatively small length scales. The time necessary to satisfy Eq. 1 is T_t, defined by Kim et al. (2010) as

$$T_t = S_x\left(\frac{\partial S_y}{\partial t}\right)^{-1} = S_x\left(\frac{\Delta\sigma}{L_y}\right)^{-1} \tag{2}$$

where $\Delta\sigma$ is the differential subsidence rate over the lateral distance L_y.

Kim et al. (2010) proposed that tectonic versus sediment dominance is controlled by overall channel mobility compared with T_t. As such, if channels are sufficiently mobile to rework the depositional surface to grade faster than the tectonic regime can tilt the depositional surface to the cross-system slope necessary for steering, the system will be channel-dominated.

The definition of the channel time scale, T_c, is not as clear as that of T_t, because in most cases channel migration has a stochastic component. One definition for T_c, however, is the time necessary for channels to migrate over the width of the basin, thus visiting every point at least once. This time scale can be estimated using

$$T_c = \frac{B_t - B_w}{v_c} \tag{3}$$

where B_t is the total basin width, B_w is the total wetted width, and v_c is a characteristic rate of lateral channel movement (avulsion plus continuous migration). The migration rate in general depends on bed-material sediment flux (Wickert et al. 2013). Paola et al. (2001) and Sheets (2004) have suggested that a rough velocity scale for channel lateral migration can be calculated using a system's width-averaged sediment discharge, q_s, and mean flow depth, h:

$$v_c = \frac{q_s}{h} \tag{4}$$

Intuitively, Equation 4 can be understood as follows: systems with high q_s have sediment available to frequently interact with channel margins that can aid lateral migration, while shallow channels need to exchange less sediment with the bed to allow for the lateral migration over a given distance. Thus systems with high sediment discharge and shallow depths should migrate laterally faster than systems with low sediment discharge and deep channels. Cazanacli et al. (2002) used a harmonic function to measure the time necessary for experimental channels to visit a given fraction of a basin. This function expresses the remaining dry fraction, f_d, in the fluvial surface at time t as

$$f_d(t) = f_d(0)\left(1 + \frac{t}{t_{rw}}\right)^{-1} \tag{5}$$

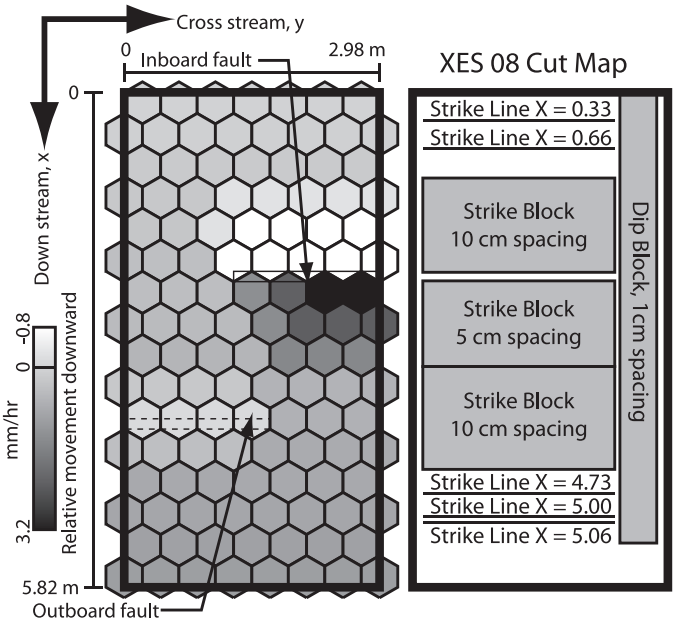

FIG. 1.—Plan view of the Experimental Earth-Scape (XES) basin showing rate and geometry of subsidence in XES 08 stage 1, including locations of inboard and outboard faults and locations of stratigraphic cross sections collected from final deposit.

where $f_d(0)$ is the dry fraction at $t = 0$ and t_{rw} is a characteristic decay time for the remaining dry fraction. Kim et al. (2010) showed that the time necessary for f_d to reach 5% was well approximated by Equations 3 and 4 for an experimental stage with no cross-stream subsidence gradient, lending support for the use of these equations in predicting channel time scales from parameters which can be measured in active systems.

Next, a time-scale ratio can be formulated using T_c and T_t:

$$T_* = \frac{T_c}{T_t} \cong (B_t - B_w)\left(\frac{q_s}{h}\right)^{-1} S_x{}^{-1}\left(\frac{\Delta\sigma}{L_y}\right) \tag{6}$$

We view T_* as a metric which can be used to define the ability of tectonics to steer channels in subsiding basins. Systems with a T_* value $>> 1$ should be tectonically dominated while systems with T_* values $<< 1$ should be channel dominated.

EXPERIMENTAL METHODS

The experiments reported here were designed to investigate the influence of lateral gradients in subsidence on surface processes and resulting stratigraphy. We use data from XES 05, originally reported on by Kim and Paola (2007) and Kim et al. (2010) in addition to a new experiment, conducted in 2008, referred to as XES 08. The subsidence pattern for both XES 05 and XES 08 was designed to represent extensional relay ramps bounded by adjacent normal fault segments (Larsen 1988; Gupta et al. 1999; Densmore et al. 2003). An inboard (upstream) fault was placed at $x = 2.2$ m and an outboard (downstream) fault at $x = 4.0$ m. A vertical wooden wall buried perpendicular to the mean flow direction inside the gravel layer acted as the inboard fault (Fig. 1). The wooden wall blocked horizontal gravel flow and thus provided a vertical surface of discontinuity in gravel movement between the downstream hanging wall and the upstream footwall. The outboard fault was less critical to the experimental design and was modeled using only changes in the subsidence rate, without a buried fault wall. The near upstream part of the inboard and outboard faults experienced relative tectonic uplift equal to 0.25 that of the maximum subsidence in the

TABLE 1.—*Experimental parameters.*

	Duration	q_s	q_w	q_s/q_w	h	$(B_t - B_w)/B_t$	T_c	S_x	$\Delta\varphi/L_y$	T_t	T_*
	hr	m^2/hr	m^2/hr	(1/1)	(m)	(1/1)	(hr)	(1/1)	(hr)	(hr)	(1/1)
XES 08: Stage 0	151	0.0035	0.35	0.01	0.01	0.67	5.7	N/A	0	∞	**0**
XES 08: Stage 1	50	0.0035	0.35	0.01	0.01	0.72	6.1	0.036	0.0026	13.8	**0.44**
XES 08: Stage 2	50	0.002	0.2	0.01	0.01	0.76	11.3	0.043	0.0026	16.5	**0.68**
XES 08: Stage 3	52	0.0014	0.14	0.01	0.01	0.73	15.4	0.053	0.0026	20.4	**0.76**
XES 05: Stage 0	185	0.0012	0.12	0.01	0.01	0.7	17.8	N/A	0	∞	**0.00**
XES 05: Stage 1	100	0.0012	0.12	0.01	0.01	0.67	17.0	0.049	0.0026	18.8	**0.90**
XES 08: Stage 4 Pulse, hrs 168–174	6	0.0014	0.14	0.01	0.01	0.85	18.0	0.057	0.0077	7.4	**2.43**
XES 08: Stage 4 Inter-Pulse, hrs 174–188	14	0.0014	0.14	0.01	0.01	0.8	17.0	0.055	0	∞	**0**
XES 08: Stage 4, hrs 168–188	20	0.0014	0.14	0.01	0.01	0.82	17.3	0.055	0.0023	23.9	**0.72**

hanging wall. The tips of the outboard and inboard faults were fixed at 1/3 and 2/3 of the basin width, generating an *en echelon* geometry. Similar to many natural systems, the displacement gradient along the inboard fault was linear (Cowie and Shipton 1998). In both XES 05 and XES 08, the extensional-relay-zone subsidence pattern was imposed following pre-experiment phases with no tectonic or base-level changes. The initial phase of XES 05 (hereafter XES 05 Stage 0) lasted 185 hr while the initial phase of XES 08 (hereafter XES 08 Stage 0) lasted 155 hr. In both experiments, the initial stage included the progradation of deltas in shallow water resulting in an initial shoreline position approximately 4.2 m from the sediment source.

The XES basin uses gravel extraction from hexagonal cells to generate basin deformation. As such, only downward tectonic motion can be produced. To generate the relative tectonic uplift, upstream of the inboard and outboard faults, we combined differential subsidence with steady base-level fall. Thus, cells that subside at a lower rate than the base-level fall rate experience relative uplift. The first and only stage completed in XES 05 (XES 05 Stage 1) included relative subsidence rates from a maximum of 3.2 mm h^1 to a minimum of 0.8 mm h^{-1}, and a background hinge-type subsidence that linearly increased from 0.0 mm hr^{-1} at the upstream end to 0.2 mm h^{-1} at the downstream end of the basin. Sediment and water feed rates were kept constant at 3.5×10^{-3} and 3.5×10^{-1} m^3h^{-1} throughout XES 05 stages 0 and 1. Sediment supply was set to balance the total accommodation creation, maintaining the shoreline at an approximately constant location through the course of stage 1. Sediment and water were mixed outside of the basin and fed from a single point source at the center of the upstream basin wall. The sediment mixture was composed of 70% quartz sand (110 μm) and 30% coal sand (bimodal: 460 and 190 μm). In XES 05 Stage 1, 5% of the total quartz sand was replaced by red-colored sand (110 μm) to allow identification of Stage 1 deposits in stratigraphic sections. XES 05 Stage 1 had a duration of 100 hr. As reported in Kim et al. (2010) the experimental design of XES 05 Stage 1 resulted in a tectonics-dominated system.

The first three stages of XES 08 were designed with the same relay-ramp subsidence pattern used in XES 05. To examine the influence of T_* on channel steering we varied the input sediment and water discharges of the three stages, while keeping the subsidence rates associated with the relay ramp constant and equal to that of XES 05 Stage 1 (Table 1). Our aim was to gradually move from sediment-dominated to tectonics dominated from stages 1–3 in XES 08. As with XES 05 Stage 1, the ratio of volumetric sediment flux, Q_s to volumetric water flux, Q_w, was kept constant at 0.01 for all stages. The only difference in the subsidence pattern between stages of XES 05 and XES 08 involved the magnitude of the background hinge-type subsidence, which was varied to balance sediment supply with total accommodation creation per stage. XES 08 stages 1, 2, and 3 had durations of 50, 50, and 52 h, respectively.

A fourth stage of XES 08 was performed to analyze the effect of pulsed slip on channel steering. XES 08 Stage 4 had identical water and sediment feed rates and rates of hinge-type subsidence as XES 08 Stage 3. The magnitude of the relay-ramp subsidence pattern and base-level fall rate, however, varied with time. XES 08 Stage 4 began with a 16 h interpulse period with no fall of relative base level and only hinge-type subsidence with no cross-stream subsidence gradient. This was followed by a 6 h period during which a relay ramp subsidence pattern, identical in geometry to previous XES 05 and 08 stages, was imposed, with relative subsidence rates that varied from a maximum of 9.2 mm h^{-1} to a minimum of 2.8 mm h^{-1}. Following the tectonic pulse, a second interpulse period with no fall of relative base level and only hinge-type subsidence was imposed for the final 24 h of the experiment. In XES 08 stages 2, 3, and 4, 5% of the total quartz sand was replaced by red, blue, and orange colored sand (110 μm), respectively, to allow differentiation of each stage's experimental deposits in stratigraphic sections. Full details of the experimental parameters can be found in Table 1.

Over the course of both XES 05 and 08 the topography of the fluvial surface was periodically measured following a well-established protocol for the XES basin that uses a subaerial laser topography scanning system. Intervals between topographic scans varied between 1 to 4 hours with topography scanned every hour during the tectonic pulse event in XES 08 Stage 4 and every two hours in the following post-pulse period. The topographic scans were gridded, with a spacing of 0.05 m in the downstream direction and 0.01 m in the cross-stream direction. Overhead digital images of the basin surface were collected every 10 s. For purposes of flow visualization, input water was dyed blue with commercial food coloring and made opaque by adding a small amount of titanium dioxide to the sediment mixture. The overhead images were post-processed to remove camera lens distortion producing images with 1 mm precision that are co-registered with the topographic scans.

After each experimental run, the deposit was sectioned to record the stratigraphy using a semiautomated deposit-cutting and imaging system designed and constructed at SAFL, which produced images with sub-millimeter resolution (Mullin and Ellis 2008). The XES 05 experiment was sliced in the dip direction every 0.01 m, for a total of 260 dip sections, each spanning the length of the basin. Sectioning of the XES 08 experiment was done at a coarser grid spacing. The XES 08 deposit was sectioned every 0.01 m in the dip direction between y locations 2.42–2.85 m. To complement the dip panels, the deposit was sectioned in the strike direction at 51 x locations between y locations of 0.12–2.36 m. The density of strike-oriented panels was highest between the inboard and outboard faults panels with panel spacing of 0.05 m (Fig. 1).

STEERING ASSOCIATED WITH STEADY SUBSIDENCE

Experimental Observations

Estimation of Tectonics and Channel Time Scales.—The formulations for the tectonic and channel time scales as defined in Equations 2 and 3

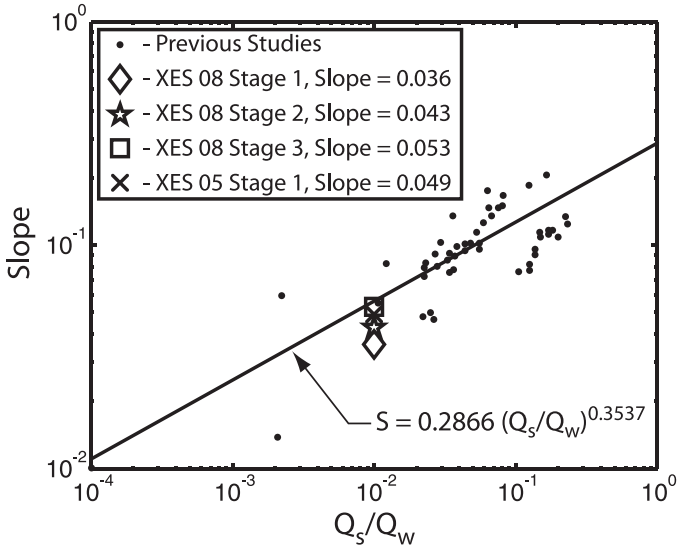

FIG. 2.—Data defining relationship between Q_s/Q_w and resulting fluvial surface slopes from compilation of experimental results originally presented in Kim et al. (2010).

each contain variables that cannot, at present, be predetermined from boundary conditions with high precision. These variables include the mean downstream slope (S_x), the mean fraction of a surface occupied by channels ($(B_t - B_w)/B_t$), and the velocity at which channels migrate over a surface (v_c). We use topographic scans and overhead images of the active fluvial surface to measure these variables, thus allowing us to estimate T_t, T_c, and T_*.

A series of papers by Parker et al. (1998a, 1998b) and Whipple et al. (1998) examined controls on transport slope for transport-limited channel and sheet-flow systems. The dominant variable identified in their experiments and analysis was the ratio of sediment discharge to water discharge, with a positive correlation between Q_s/Q_w and transport slopes. Kim et al. (2010) compiled data on transport slope from a range of experiments spanning a wide spectrum of Q_s/Q_w and found a similar correlation with considerable scatter in the trend (Fig. 2). Using the relationship presented in Kim et al. (2010) we would predict $S_x = 0.056$ for a Q_s/Q_w of 0.01. As the highest cross-stream gradient in subsidence rate occurs in the relay zone ($2 \text{ m} < x < 3$ m), we focus our characterization of S_x on this region (Fig. 3A). We find that S_x varied between 0.034 and 0.056 over the course of the two experiments. While some variability in slope existed within any one stage, the autogenic variability was far exceeded by the variability between individual stages. In general, we note an increase in transport slope inversely correlated with the absolute magnitudes of Q_s and Q_w (Table 1).

Given the dependence of S_x on the absolute magnitude of Q_s and Q_w we calculate two time scales associated with a transport system adjusting S_x in response to a change in boundary conditions. This is done in an effort to identify periods in the experiment during which transport slopes are adjusting to changes in boundary conditions, and as such, should be excluded from our analysis. First, we define a time necessary for a system to regrade S_x, assuming all available Q_s goes solely to slope adjustment

$$t_{regrade} = \frac{B_t L_x{}^2 \left(S_{x,t=i} - S_{x,t=final}\right)}{Q_s} \tag{7}$$

where L_x is the length of the transport system, $S_{x,t\,=\,i}$ is an initial slope and $S_{x,t\,=\,final}$ is the final transport slope. We note that this is a minimum time scale for slope adjustment as some sediment is stored via accommodation associated with basin subsidence. Using Eq. 7 we calculate $t_{regrade}$ values of 6.9 and 18.2 h for the transitions between XES 08 stages 1–2 and XES 08 stages 2–3, respectively. A second time scale used to analyze system adjustment to a change in boundary conditions is the basin equilibrium time (Paola et al. 1992), t_{EQ}, defined as

$$t_{EQ} = \frac{L_x{}^2}{v} \tag{8}$$

where v is the transport coefficient of a system, estimated as

$$v = \frac{Q_s}{B_t S_x} \tag{9}$$

Using Equations 8 and 9, we calculate t_{EQ} values of 283 and 483 h for the XES 08 stage 1–2 and XES 08 stage 2–3, respectively. While these t_{EQ} values are significantly longer than individual stage durations, numerical modeling and field observations demonstrate that most fluvial adjustment occurs well before a system achieves complete equilibrium following a perturbation (Snow and Slingerland 1990; Shen et al. 2012). Because S_x and S_y appear to come into dynamic equilibrium following $t_{regrade}$ and well before t_{EQ}, we analyze data only from stages 2 and 3 of XES 08 for the portion of stages that exceed $t_{regrade}$. Thus we are ignoring portions of the experiment during which the transport system was dominantly responding to changes in boundary conditions. The deposition of sediment associated with slope increases during stage transitions resulted in transgressions of the shoreline at the beginning of XES 08 stages 2 and 3, most noticeably downstream of the maxima in subsidence.

Next, we estimated the average wetted fraction, $(B_t - B_w)/B_t$, of the delta top in all experimental stages using the overhead images of the active transport system. Using a threshold blue color value, determined from visual inspection, we separated dry regions from wet regions on the delta top. A time series of wetted fraction for the two experiments shows considerable variability within any one stage (Fig. 4). This intrastage variability exceeds the magnitude of variability in the mean wetted fraction between stages. Calculated mean wetted fractions for individual stages were all between 0.67 and 0.8 with no trend with respect to the absolute magnitudes of Q_s and Q_w (Table 1).

The final variable necessary to estimate T_t, T_c, and T_* is channel depth. Based on the idea that it is the deep scours that matter most for stratigraphy (Paola and Borgman 1991), we instead estimate the mean depth of channel scours from measured topography and the resulting thickness of channel bodies preserved in the stratigraphy. While considerable variability is observed throughout all experimental stages, we do not see a detectable difference in the mean channel-scour depth or preserved channel-body thickness between stages and thus use a constant measured value of 0.01 m for all stages.

We now have estimates of all necessary variables for estimating T_t and T_c, with the results detailed in Table 1. We make the following observations: 1) For the experimental parameters in XES 08 stages 1–3 and XES 05 Stage 1, which included equivalent relay-ramp subsidence geometry and rates, we observed a decrease in tectonic time scale as the magnitude of sediment and water feed rates into the basin increase. This is due to the decrease in S_x as Q_s and Q_w increased. 2) We observe a decrease in channel time scale as the magnitude of sediment and water flux into the basin increase. We use our calculations of T_c and T_t to estimate T_* values of 0.44, 0.68, 0.76, and 0.90 for XES 08 stages 1–3 and XES 05 Stage 1, respectively.

Measuring Surface Reworking Time.—While Equation 3 allows us to estimate T_c for our experimental stages, we are interested in comparing these estimates with measurements of the time associated with channel migration over all or most of the basin surface. To accomplish this, we use Equation 5 in conjunction with our overhead photos of the active

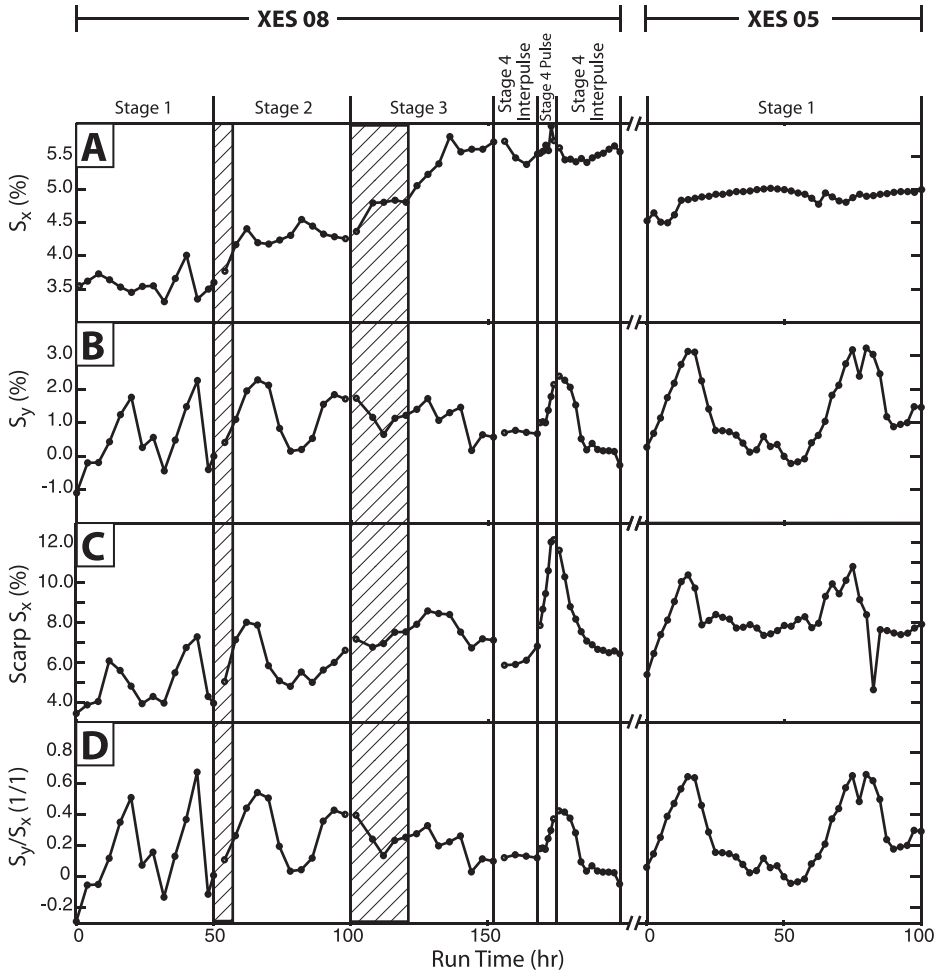

FIG. 3.—Time series of various components of surface slope measured from topographic surveys collected during XES 05 and 08. **A)** Time series of down-stream surface slope, S_x, measured in the relay-ramp zone ($2\text{ m} < x < 3\text{ m}$), **B)** time series of cross-stream surface slope (positive sloping towards river-left wall), S_y, measured in the relay-ramp zone ($2\text{ m} < x < 3\text{ m}$), **C)** time series of down-stream surface slope measured in the region of the inboard fault ($2\text{ m} < x$ 2.4 m and $1.5\text{ m} < y < 3\text{ m}$), **D)** time series of S_y/S_x ratio. Hashed region denotes time for slope adjustment predicted by Eq. 8.

surface to quantify dry-fraction reduction time scales. Using the method we used to calculate wetted width, we generate wet–dry maps of the experimental surface for every minute of the two experiments. We track dry-fraction reduction by monitoring the fraction of area yet to be visited by flow for 10 hour windows, starting every 0.5 hr of run time in the two experiments. The measured decay of $f_d(t)$ is then fitted with Equation 5 to produce an estimate of t_{rw} and $t(f_d = 5\%)$, the time necessary for flow to visit 95% of the basin surface. A time series of $t_{95} = t(f_d = 5\%)$ for the two experiments is shown in Figure 4C. It leads to the following observations: 1) In all experimental stages t_{95} fluctuates between periods of low channel migration (correlated in time with flow over the upstream region of uplift (Fig. 4B)), and periods of rapid channel migration (correlated in time with periods following surface being brought to grade (*sensu* Mackin 1948)). 2) The character of t_{95} time series in XES 08 stages 0 and 1 appear visually similar, while XES 05 Stage 1 displays larger peaks in t_{95} when compared to XES 05 Stage 0. In both experiments, Stage 0 had identical water and sediment feed conditions as Stage 1, but Stage 0 lacked spatially varying subsidence. 3) As T_* increases, the magnitude of peaks in t_{95} for a given stage increase.

Next, we use time series of t_{95} to estimate a mean t_{95} for each experimental stage (Table 2). As highlighted in Figure 5A as well as Figure 4C the decay of f_d within any one stage shows tremendous variability. However, when averaging this variability we find the following results. As T_* increases, the mean t_{95} for a stage also increases (Fig. 5B, Table 2). Second, when comparing XES 08 Stage 1, with a T_* of 0.44, to XES 08 Stage 0, we find that the addition of spatially varying tectonics with this T_* increases t_{95} by only 1%. However, comparing XES 05 stages 0 and 1 we find an increase in t_{95} of 97% through addition of spatially varying tectonics when T_* equals 0.90. As such, it appears that the addition of spatially variable subsidence in tectonics-dominated settings (relatively high T_*) influences channel kinematics through a reduction of channel mobility, i.e., a positive feedback that enhances steering, while channel mobility is unaffected by spatially variable subsidence in sediment-dominated systems (low T_*).

Steering through Flow Rotation.—In the remainder of this paper we differentiate two types of channel steering: 1) short-term deflection or rotation of channels in plan view toward subsidence maxima associated with the development of cross-stream slopes and 2) long-term preference for channels to occupy a particular location in a basin. We differentiate these two types of steering because short-time-scale steering can occur due to lateral subsidence gradients without causing a long-term preference for flow to occupy sites over the subsidence maximum. As we discuss below, short-lived steering events can be erased quickly enough that they do not create long-term preferential flow occupation over subsidence maxima. We start by examining the first definition as it relates to our experiments. Three of the four steady-deformation stages (XES 08 stages 1 and 2 and XES 05 Stage 1) showed a similar cycle in surface flow configuration, described below and in Kim et al. (2010). Following a period of autogenic migration of flow towards the river-right side of the basin, when viewing the flow as moving from source to sink, the region of maximum subsidence became underfilled with sediment. As a result, a cross-stream slope, S_y, developed in the direction of the subsidence maximum (Fig. 3B), which to varying degrees drew flow towards the subsidence

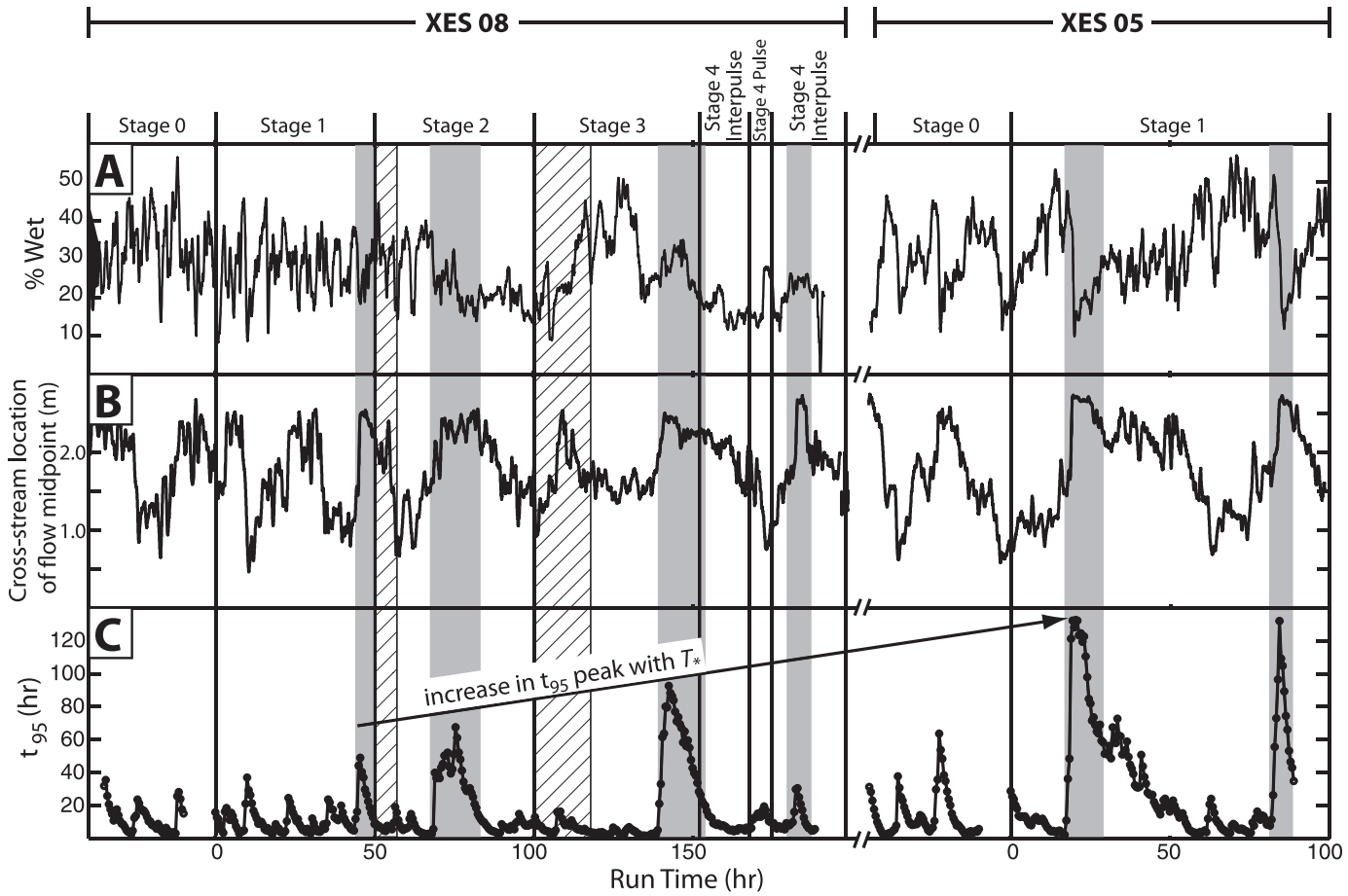

FIG. 4.—Time series of parameters characterizing the lateral extent, location, and mobility of experimental channels. **A)** Time series of percent of delta top area occupied by surface flow captured from overhead images. **B)** Cross-stream location of center of channelized flow. **C)** Time series of $t(f_d = 5\%)$ calculated from decay of dry fraction initiated every 0.5 hours of experiment. Hashed region denotes time for slope adjustment predicted by Eq. 8. Gray regions highlight periods associated with peaks in $t(f_d = 5\%)$ for each stage.

maximum (Fig. 6A, D, G). At this time, a surface scarp formed at the inboard fault (Fig. 3C). This pattern persisted until a cross-stream slope developed, due to sedimentation upstream of the inboard fault, that routed flow directly over the inboard region of uplift and into the subsidence maximum (Fig. 6B, E, H). Routing of flow over the upstream region of uplift was associated with focused erosion of sediment, which then was deposited, primarily as lobes in the subsidence maximum, returning this region to grade. Once the system was returned to grade a new period of autogenic channel migration began (Fig. 6C, F, I), which lasted until an autogenic migration of flow towards the river-right side of the basin started the cycle anew. While this full cycle was not observed in XES 08 Stage 3, the first two phases of the cycle were observed and the third phase possibly could have occurred if the stage had been run for a longer duration.

While the cycle of 1) cross-system channel steering into the subsidence maximum, followed by 2) focused erosion and filling of below-grade topography and ending with 3) a new autogenic migration phase, was at least partially developed in all experimental stages, we note an increase in the period of this cycle with T_*. We estimated cycle periods of 20 ± 5hrs, 28 ± 5hr, and 52 ± 5hrs for T_* values of 0.44 (XES 08 Stage 1), 0.68 (XES 08 Stage 2), and 0.90 (XES 05 Stage 1), respectively. This increase in cycle period allowed larger topographic depressions to form as T_* increased, thus increasing the magnitude of channel steering. This trend is particularly apparent in XES 05 Stage 1, where an autogenic lake formed as a result of the long cycle period (Kim et al. 2010). We also emphasize here that in all experimental stages, this autogenic cycle resulted in at least brief periods in which the flow was visibly deflected into the subsidence maximum.

Finally, we use our time series of topographic surveys to examine the Hickson et al. (2005) hypothesis that the ratio of S_y to S_x must be order 1 or greater for steering to occur through flow deflection. To do this we use our estimates of S_x and S_y from topographic surveys. Our first observation is that at no time in the two study experiments did the ratio of S_y/S_x equal or exceed unity (Fig. 3D). This implies that for all stages, channel mobility was great enough to at least partially rework surface topography over a time window less than T_t. However, steering of channels towards the subsidence maximum was frequently observed, particularly in XES 05 Stage 1. Periods of channel steering through flow deflection appeared to occur when S_y/S_x exceeded a value of approximately 0.5.

Steering through Preferential Flow Occupation.—Using the wet–dry maps generated for each 1 minute of the two experiments we generate maps of the fraction of time that flow occupied each location in the basin. These maps help identify regions with enhanced flow occupation and avoidance relative to what would be expected from random channel migration in the basin. Given the basin feed location at the center of the upstream wall, we would expect near-uniform flow occupation at all

TABLE 2.—*Estimate of time necessary for flow to rework surface.*

Experiment	Stage	t(f_d = 0.05) (hr)
XES 08	0	14.1
XES 08	1	14.2
XES 08	2	19.3
XES 08	3	21.5
XES 05	0	17.7
XES 05	1	34.9

locations in the basin, with a possible slight preference for occupation near the center of the basin along any one strike-oriented transect if flow migrated randomly. However, in maps of flow occupation, presented in Figure 7, we observe an increase in the fraction of time in which flow occupied the zone of subsidence maximum as T_* increased. To characterize a most-frequent flow path we identified the cross-stream location with the highest flow occupation for each downstream distance in each stage (identified as gray circles in Fig. 7). In XES 08 Stage 1 the most-frequent flow path, while displaying some cross-stream variability, roughly runs down the center of the basin. In XES 08 Stage 2 we observe a most-frequent flow path that runs along the basin center line above the inboard fault, then is deflected towards the subsidence maximum. In XES 08 Stage 3 and XES 05 Stage 1 we observe most-frequent flow paths that are deflected over the upstream zone of uplift, cutting across the inboard fault and into the subsidence maximum. The preference for flow occupation over zones of high subsidence suggests steering related to the spatially varying subsidence field.

Given the considerable variability in cross-stream location of maximum flow occupation, we produced average cross sections of flow occupation for the zone upstream of the inboard fault (x = 1.6–2.1 m) and for the relay zone (2.5–3.0 m) (Fig. 8). With the exception of XES 08 Stage 3, we find no cross-stream trend in channel occupation upstream of the inboard fault. XES 08 Stage 3 shows a dominant peak in channel occupation over the region of uplift, associated with incisional stabilization of flow across the uplift. In the relay zone, a trend of increasing flow occupation towards the subsidence maximum as T_* increases is observed, indicating an increase in channel steering with T_*.

Stratigraphy

Given the equivalence of input Q_s and accommodation creation in individual stages of XES 05 and XES 08, and the relatively high mobility of channels in both experiments, it should not be surprising that the final deposit shapes in the two experiments match the subsidence pattern. To examine differences in stratigraphy between experimental stages we take advantage of the differing colors of the supplied sediment in each stage and measurements of topography. As previously discussed, 5% of the white quartz sediment in XES 08 stages 2–4 and XES 05 Stage 1 was replaced with quartz sediment dyed red, blue, orange and red, respectively. Synthetic stratigraphic time lines were generated through stacked delta-top profiles with topography migrated to account for basin subsidence and then clipped to account for sediment removed during erosion (Martin et al. 2009). Images of preserved physical and synthetic stratigraphy are displayed in Figures 9 (dip transects) and 10 (strike transects). Preserved channel scours are visible as high-curvature features in the stratigraphy. In the dip and strike panels, we note a decrease in preservation of channel-scour features with increase in T_* in the region of high subsidence in the relay zone. In the relay zone an increase in sheet and lobe deposits compensates for the loss of channel scours in the deposit as T_* increases.

In addition to the change in channel density, the most notable stratigraphic features in the two experiments include upstream to downstream transitions in the sand–coal boundary. In the deposit associated with XES 08 stages 1–3 we note two prevalent locations where the sand–coal boundary migrates updip prior to migrating back downdip, as one moves up section. These transgressions in the sand–coal boundary occurred at the beginning of XES 08 stages 2 and 3, respectively, and likely are associated with shoreline transgression driven by slope increases at the start of each stage. Two similar transgressions of the sand–coal boundary are visible in the XES 05 Stage 1 stratigraphy.

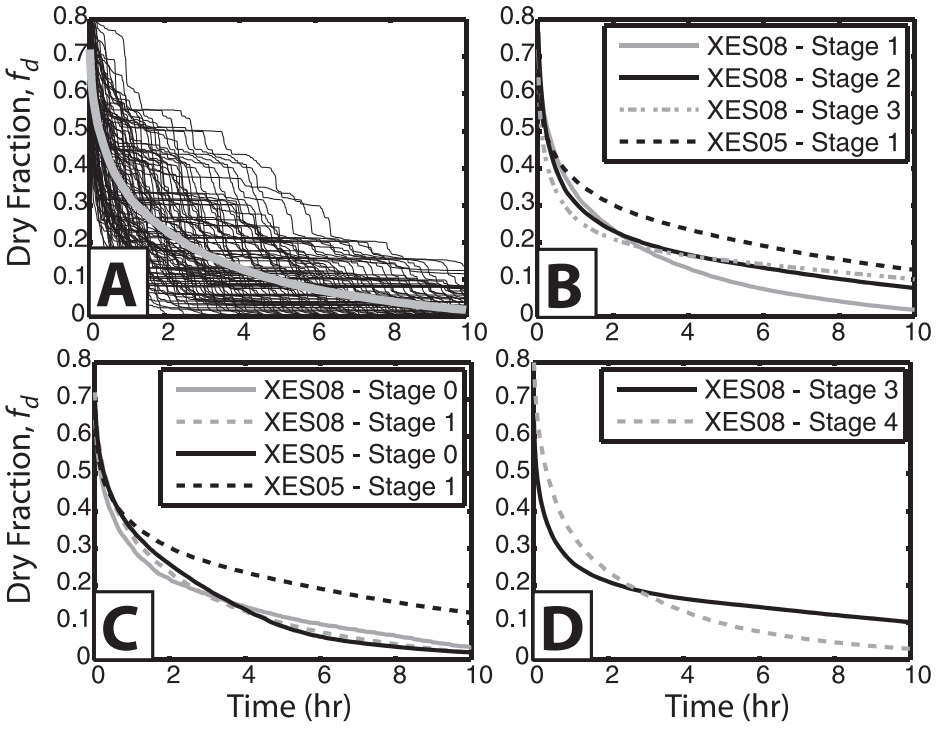

FIG. 5.—Data defining the reduction in the remaining dry fraction of the fluvial surface. **A)** 100 reduction curves, each including every 1 min measurements for 10 hr collected during XES 08 stage 1 (thin black lines) and the average remaining dry-fraction curve for XES 08 stage 1 (thick gray line). **B)** Comparison of averaged reduction of remaining dry-fraction curves as a function of T_*. **C)** Comparison of averaged reduction of remaining dry fraction curves for input Q_s and Q_w conditions with and without laterally varying subsidence gradients. **D)** Comparison of averaged reduction of remaining dry-fraction curves for stages that share similar T_* values with and without pulsed tectonics.

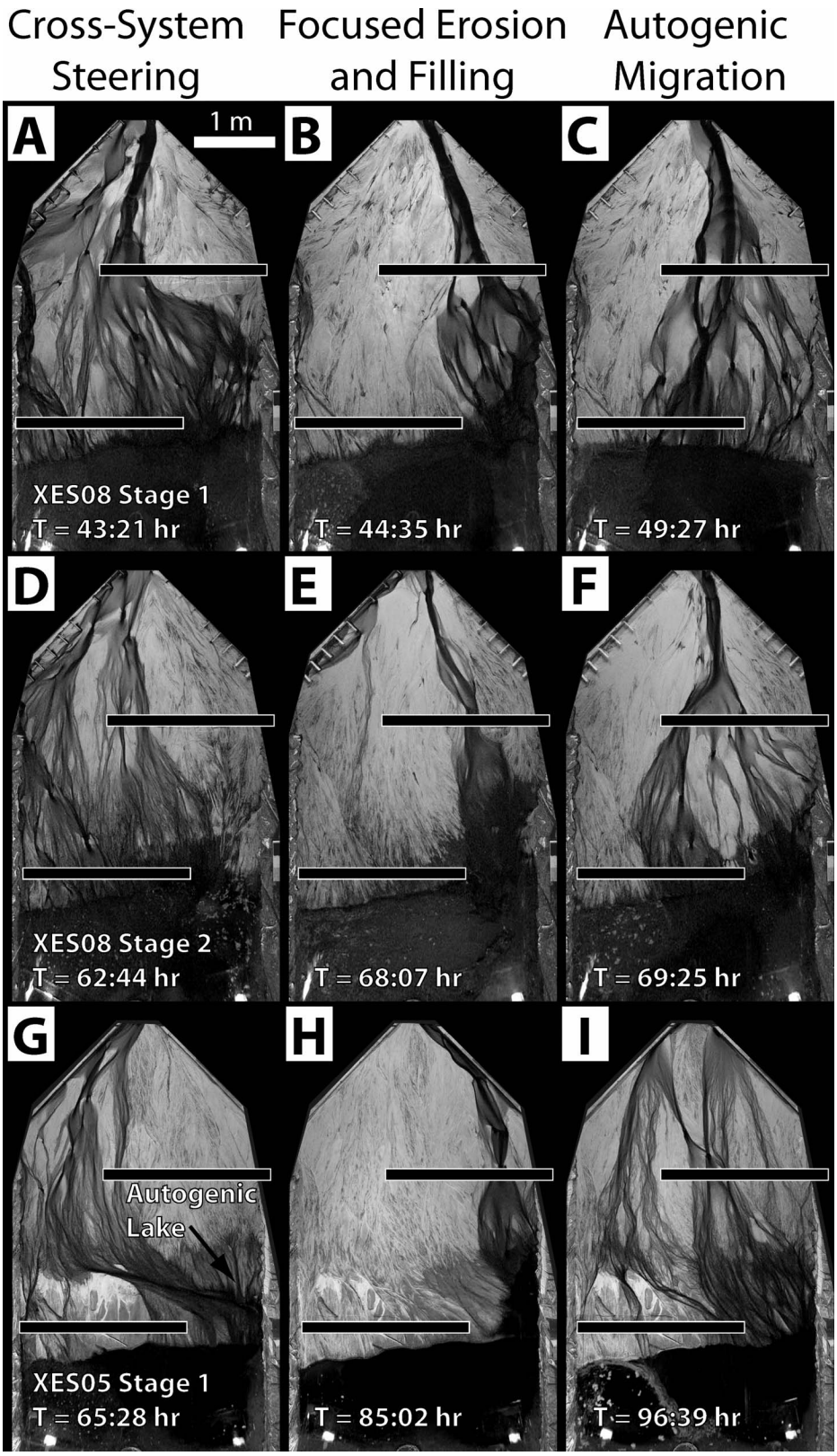

FIG. 6.—Overhead images of fluvial surface defining cycle of 1) cross-system channel steering into the subsidence maximum, 2) focused erosion and filling of below-grade topography, and 3) autogenic channel migration during XES 08 stage 1 (A–C), stage 2 (D–F), and XES 05 Stage 1 (G–I). Location of inboard and outboard faults are shown by black rectangles.

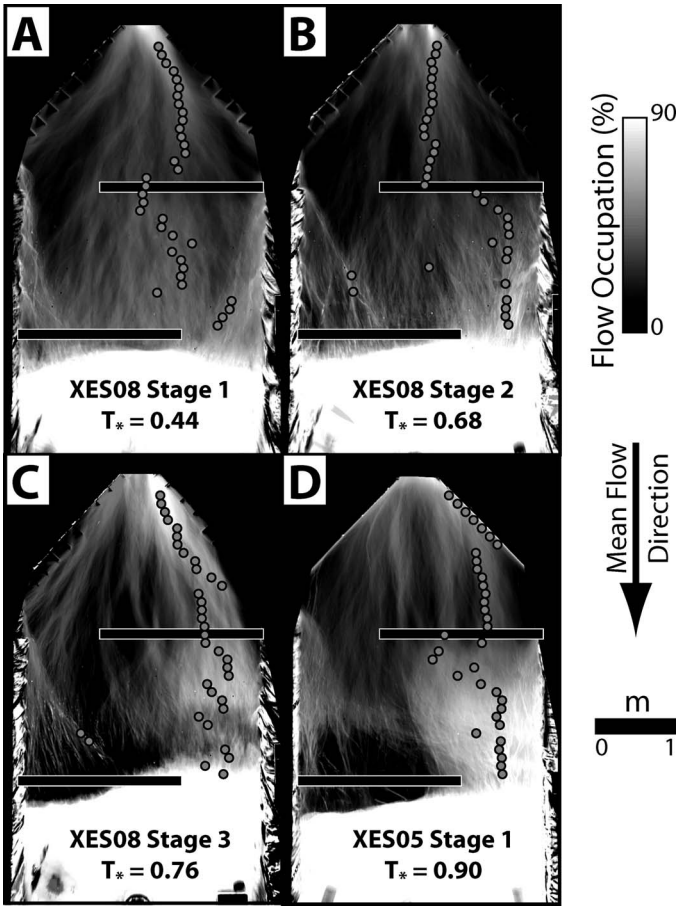

FIG. 7.—Time-integrated flow-occupation maps for complete aseismic experimental stages. White denotes continuous occupation over the full experimental stage, whereas black denotes no flow occupation. White circles denote cross-stream maximum in flow occupation for cross-stream sections sharing constant x distance from source, spatially averaged at 0.1 m increments in the x direction. Location of inboard and outboard faults are shown by black rectangles.

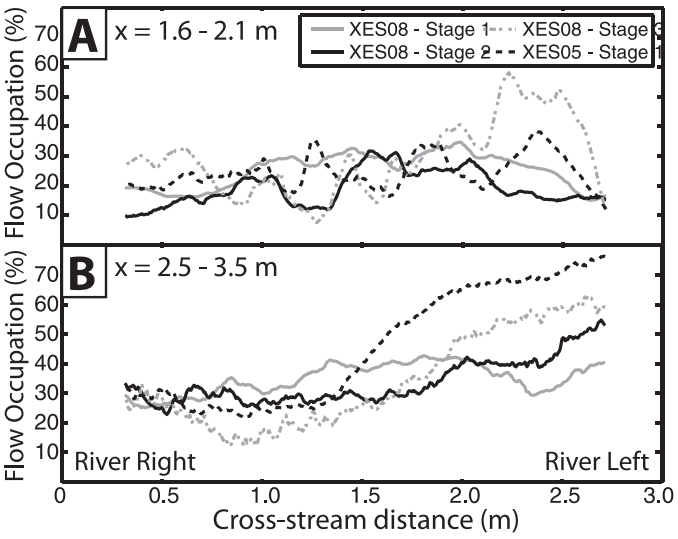

FIG. 8.—Time-integrated flow occupation **A)** immediately upstream of the inboard fault and **B)** in the relay ramp zone.

Unlike XES 08, however, these transgressions are not temporally linked to stage changes, but are linked to autogenic lake formation and filling (Kim and Paola 2007).

Interpretation

Observations from the XES 99, 05, and 08 experiments show a correlation between T_* and the strength of channel steering through lateral subsidence gradients in alluvial basins. Through our analysis of overhead images of the active surface we link the following surface processes to relay-ramp tectonics: 1) deflection of channel orientation towards subsidence maxima, 2) preference for channel occupation in subsidence maxima, and 3) decrease in channel mobility, especially in incisional zones associated with relative uplift.

Steering through Flow Rotation.—We observe periods of flow deflection, upwards of 90° relative to the dominant long-term flow direction, in both XES 08 stage 1 (T_* = 0.44) and XES 05 stage 1 (T_* = 0.90) (Fig. 6). In both of these stages, deflection of flow was associated with S_y/S_x values of approximately 0.5–0.6 in the relay zone. Thus it appears that even in settings characterized by low values of T_*, stochastic autogenic migration of channels and associated deposition occasionally allows development of surface gradients necessary for flow rotation. We do, however, note an increase in the fraction of time where flow rotation is observed as T_* increases (Supplemental Movie, see Acknowledgments). In the low T_* stages, channels swept over surfaces rapidly, and thus periods of flow deflection were significantly shorter in duration compared to the high T_* stages, as aggradation during one period of duration T_c was minimized. Development of sufficient S_y/S_x values to cause flow deflection was associated with migration of channels towards the river-right side of the basin, which resulted in reduced deposition rates in the subsidence maximum. There likely is a lower limit for a basin T_* necessary to induce flow deflection via subsidence gradients. We note that flow deflection in excess of approximately 30° relative to the dominant flow direction was not observed in XES 08 stage 0 or XES 05 stage 0, both of which lacked cross-stream subsidence gradients (Supplemental Movie).

The ability of lateral gradients in subsidence to steer flow through deflection into subsidence maxima, given sufficiently high basin T_*, should also be recorded in basin stratigraphy through paleo–flow indicators. Variability in flow direction present in active systems (Peakall 1998) and recorded in paleo–flow indicators from ancient systems (Price and Scott 1991; Leeder et al. 1996; Dorsey and Umhoefer 2000) is common and often related to stochastic channel migration and the presence of meander loops. While such autogenic processes cause variability of flow directions in basins, our results suggest that a statistical preference for flow rotation towards subsidence maximum is likely related to lateral gradients in subsidence. We emphasize, though, that a T_* value of 1 is not necessary for deflection of flow towards a subsidence maximum, as this was observed in our experiments during a stage with T_* = 0.44.

Steering through Preferential Flow Occupation.—Next, we focus on the ability of lateral gradients in subsidence to cause long-term preferences in channel occupation. In the four steady-subsidence stages we saw a consistent increase in the preference for channels to occupy locations over the subsidence maximum in the relay zone as T_* increased (Figs. 7, 8). Starting with XES 08 stage 1 (T_* = 0.44), we observe no preference for channel occupation over the subsidence maximum in the relay zone relative to other lateral locations. This lack of preference for channel occupation over the subsidence maximum occurs, even though periods of significant flow rotation were observed in this stage. As T_* increases, flow occupation maps reveal two outcomes: 1) a preference for channel

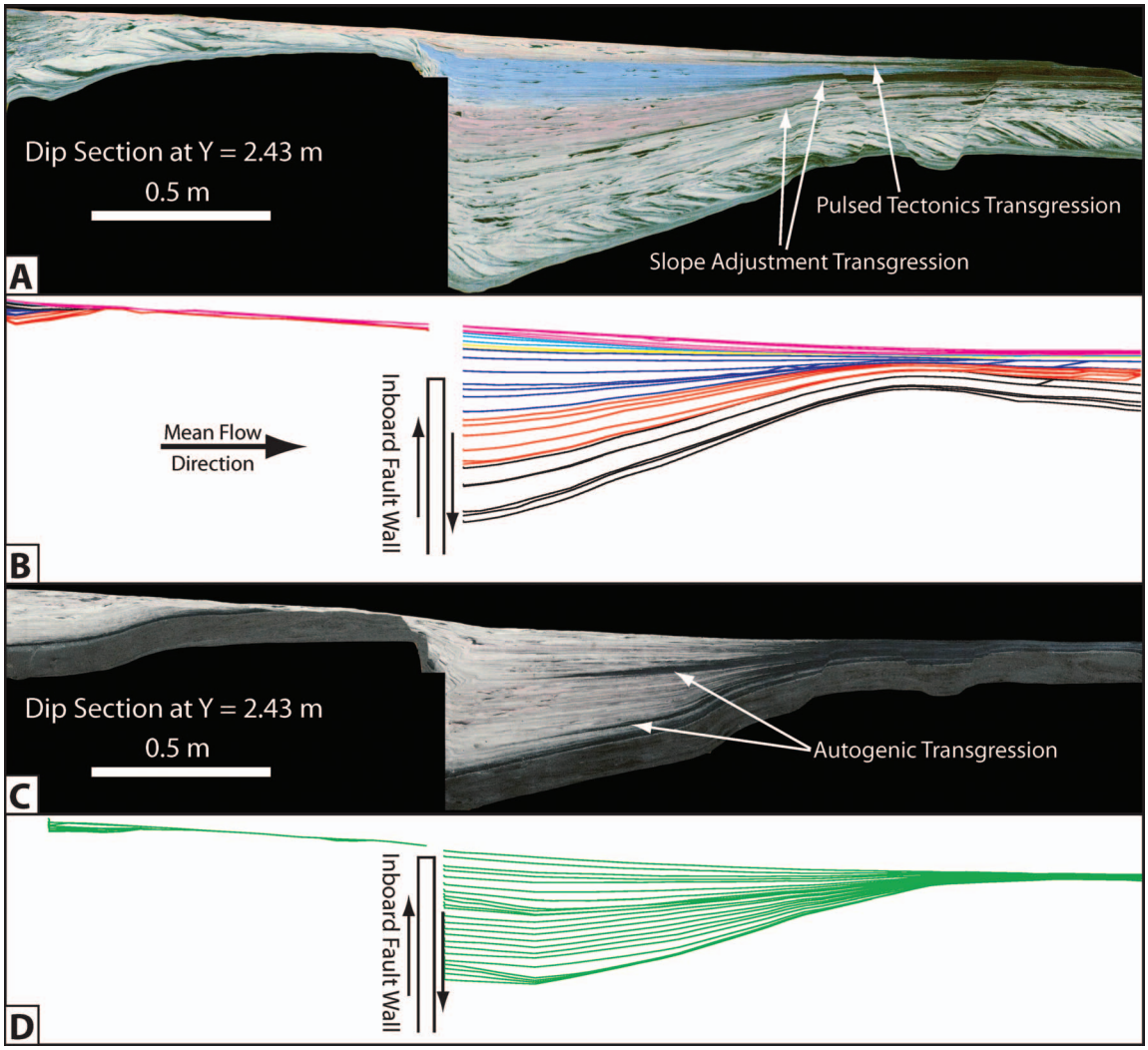

FIG. 9.—Dip sections of experimental deposit sliced in the downstream direction at $y = 2.43$ m of the **A)** XES 08 experiment and **B)** XES 05 experiment, and their associated strata geometry generated through stacked delta-top profiles with topography migrated for subsidence and clipped to account for sediment removal during erosional events.

occupation over the subsidence maximum in the relay zone and 2) a preference for flow occupation over the region of uplift upstream of the inboard fault. The first of these outcomes is consistent with the theory of Hickson et al. (2005) and Kim et al. (2010). We note that a preference for flow occupation in the subsidence maximum was observed for XES 08 stage 2 ($T_* = 0.68$), so the threshold to cause preferential flow occupation through lateral subsidence gradients lies between T_* values of 0.44 and 0.68. Kim et al. (2010) developed a means to estimate the minimum basin tilting rate necessary to induce steering by basin tilting. This was done by rearranging our Eq. 6 to solve for tilting rate while assuming a T_* of unity:

$$\frac{\Delta\sigma}{L_y} = \frac{q_s S_x}{h(B_t - B_w)} \tag{10}$$

Our observations suggest that the strength of steering gradually increases as the value of T_* increases. This steering appears to become strong enough, such that its impact can be quantified over natural autogenic variability in the transport system at $T_* \cong 0.5$, a value half of that assumed in Equation 10.

The increased preference for flow occupation over the region of uplift as T_* increases is surprising, in that this suggests that lateral gradients in basement motion have opposite effects on the steering of channels depending on whether the motion is associated with uplift or with erosion. In regions with only relative subsidence, channels are drawn to the subsidence maximum, but in regions with uplift and subsidence, flow more frequently occupies zones of uplift relative to zones of subsidence. This preference for flow occupation over the inboard uplift is temporally related to incision and reduction in channel mobility (Fig. 4). Using wet maps of the active surface, we calculated the cross-stream mid-point of flow in the downstream region of the inboard fault ($x = 1.9$–2.3 m). We find that periods of reduced channel mobility (periods of high t_{95}) occur when flow is over the region of maximum uplift ($y = 2.0$–3.0 m). During these time periods deep incisional channels formed over the uplift and eroded sediment that was transported into the subsidence maximum. These deep erosional channels migrate laterally more slowly than net-depositional channels. On long time scales, the low lateral migration rate of these erosional channels result in a preference for channel occupation over zones of uplift. This enhanced occupation over the inboard fault and zone of uplift also has the effect of temporarily focusing flow into the

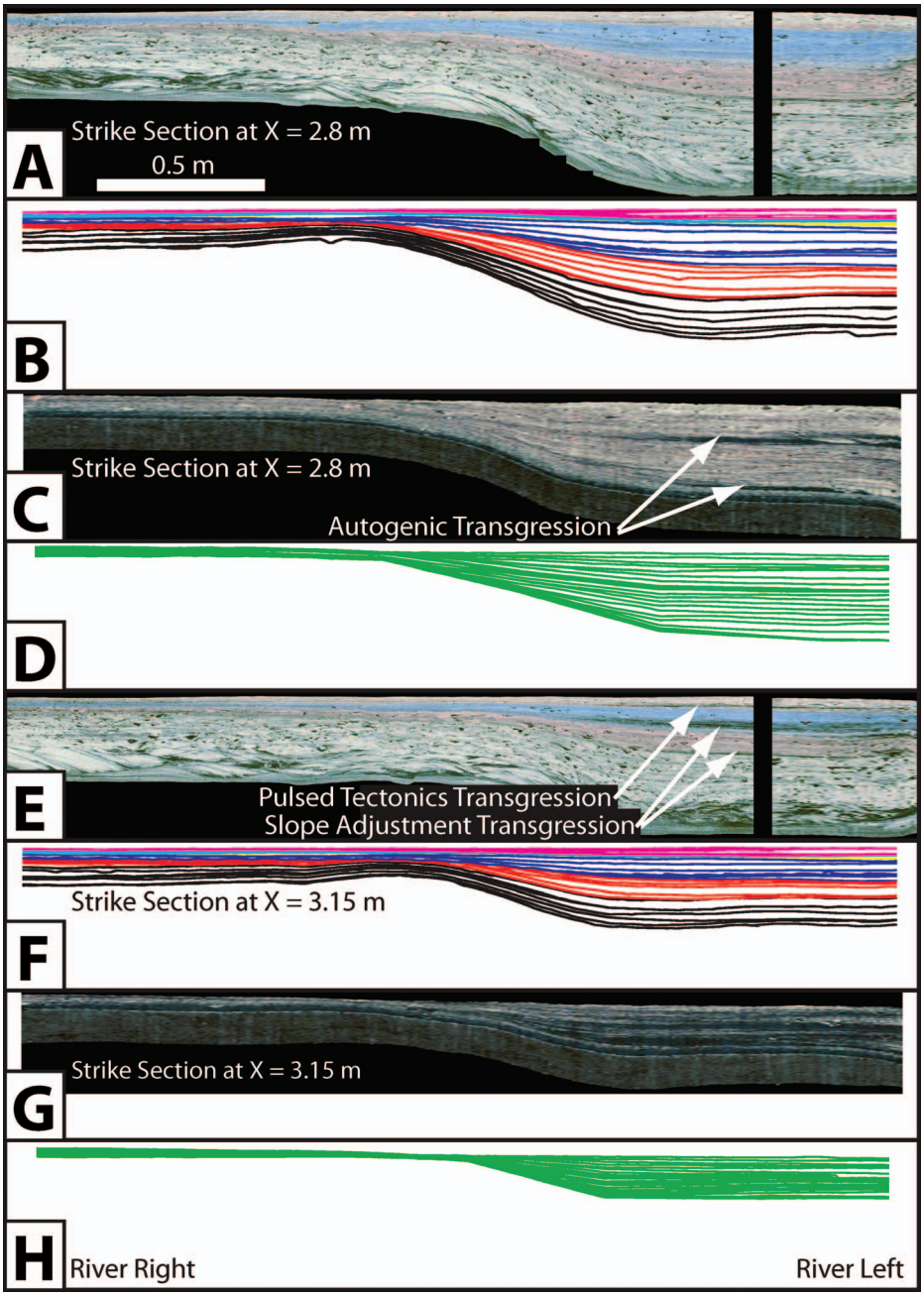

FIG. 10.—Strike sections of experimental deposit sliced in the cross-stream direction at x = 2.8 m and 3.15 m of the **A**, **C)** XES 08 experiment and **B**, **D)** XES 05 experiment, and their associated strata geometry generated through stacked delta-top profiles with topography migrated for subsidence and clipped to account for sediment removal during erosional events.

subsidence maximum via a shorter and less tortuous path than the one that follows the relay ramp. As such, part of the enhanced occupation over the subsidence maximum is due to updip focusing of flow and reduced lateral mobility when flow is centered over the uplift, and not just to rotation into the subsidence maximum. While steering of flow is commonly linked to flow deflection (particularly in relay-ramp settings, e.g., Densmore et al. 2003), we recognize this erosional focusing of flow as a second type of flow steering. We suggest that this effect is even more prevalent in natural systems associated with uplift of consolidated bedrock (e.g., Gupta et al. 1999; Densmore et al. 2003) that would be less susceptible to lateral erosion by migrating channels than the unlithified sediment that underwent relative uplift in our experiments. In regions with uplift of consolidated bedrock, upstream sedimentation likely influences the potential of channels to cross, and become spatially locked within, uplifting regions, as suggested by Humphrey and Konrad (2000). Interestingly, here we do not note any long-term enhancement of sedimentation upstream of the inboard fault that might lead to a reduction in channel mobility. Periods of enhanced deposition upstream of the inboard fault are observed over short time intervals, on the scale of 4–8 hr, but analysis of isopachs indicate that on the time scale of the duration of individual stages deposition and erosion patterns strongly mimic generation of accommodation space. On these long time scales, channel migration brings the transport system to grade frequently enough to liberate sediment, stored on the short term, upstream of the inboard fault. This suggests that the process of erosion, even of unlithified sediment, induces a reduction in channel mobility relative to channels in net-depositional settings.

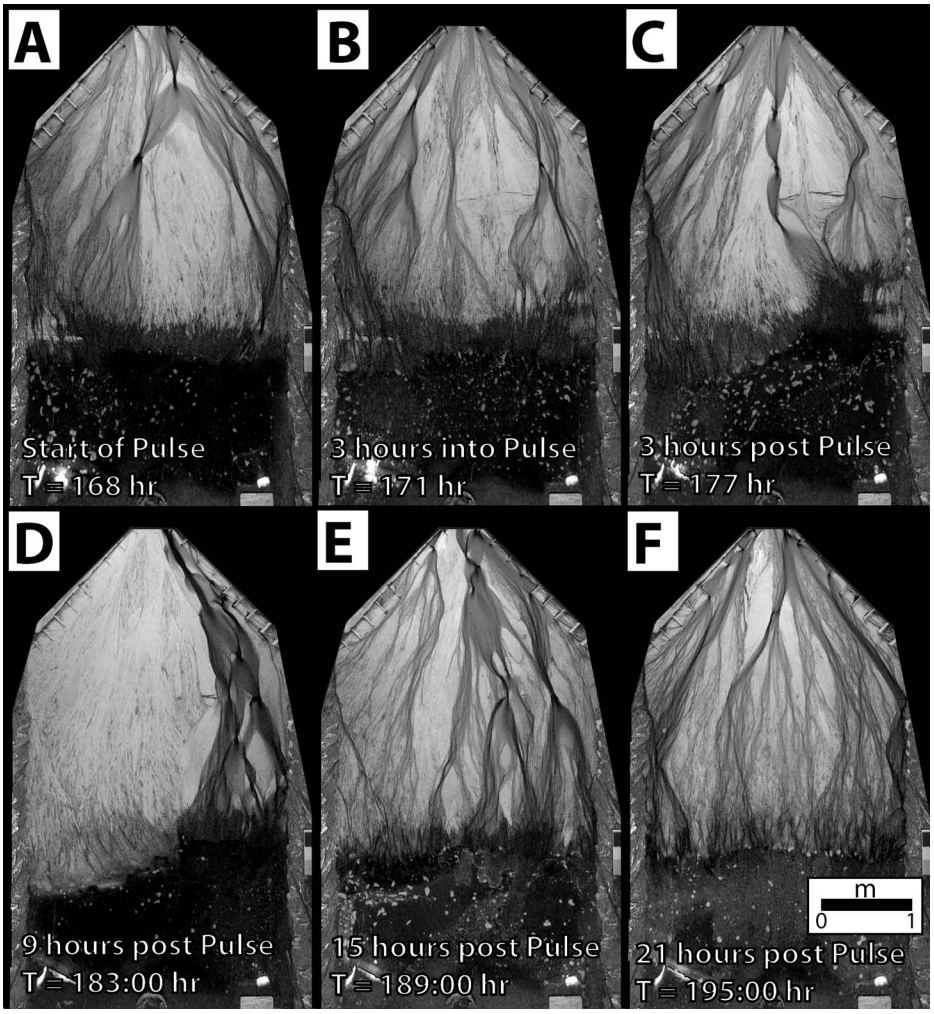

FIG. 11.—Overhead images of fluvial surface defining response of channels to **A)** subsidence pulse and **B–F)**the following interpulse–recovery period. Images are presented every six hours of pulse–interpulse cycle.

STEERING ASSOCIATED WITH PULSED SUBSIDENCE

Experimental Observations

Analysis of Tectonic and Channel Time Scales.—We extend the hypothesis of Hickson et al. (2005) to predict when subsidence pulses can steer channels and influence resulting stratigraphy. To discuss pulsed subsidence events we first define two time scales that characterize the duration, T_p, and recurrence interval, T_{pc}, of pulse events. The ratio T_p/T_{pc} defines the fraction of time a system is tectonically active over one complete pulse–interpulse sequence. Next we differentiate between a "long" tectonic time scale ($T_{t,long}$) and a "short" tectonic time scale associated with a pulse event ($T_{t,pulse}$). $T_{t,long}$ characterizes the tectonic environment over one pulse–interpulse cycle, while $T_{t,pulse}$ characterizes the tectonic time scale during one pulse event. As with steadily subsiding basins, we hypothesize that steering of channels occurs only if Eq. 1 is satisfied. In basins with pulsed subsidence, this requires that two conditions be met. First, T_* for a pulse event must be order 1 or greater. Second, we hypothesize that

$$T_{t,pulse} \gtrsim T_p \tag{11}$$

As a result, pulse events that do not last long enough to impart a cross-stream surface slope on order of the downstream slope will not steer channels, and vice versa.

We estimate T_{*pulse} for the period of pulsed tectonics in XES 08 Stage 4 as 2.43. For convenience when comparing steady and pulsed subsiding cases, we define a seismic cycle for XES08 Stage 4 as including the pulse event (hr 168–174) and 16 hr of interpulse activity (e.g., hr 174–188). This combination of pulse–interpulse activity results in a composite $T_{*pulse-interpulse}$ of 0.72, similar in magnitude to XES 08 Stage 3.

Steering through Flow Deflection.—Following 16 h of surface evolution with no lateral subsidence gradients, we imposed a period of pulsed subsidence at hour 168 of XES 08 Stage 4. At the start of the pulse, flow was split between the river-right and river-left sides of the basin with significant flow over the inboard zones of uplift and subsidence maximum (Fig. 11A). During the six hours of pulsed subsidence, flow continued to occupy portions of both the river-right and river-left sides of the basin, though there was a trend of increasing flow towards the river-right side of the basin with time (Fig. 11B). During the pulse a cross-stream slope developed in the relay zone towards the subsidence maximum (Fig. 3B) and a significant topographic scarp formed at the inboard fault (Fig. 3C). In addition, the shoreline transgressed during the pulse as a topographic low was created in the subsidence maximum. While the pulse–interpulse cycle was designed to balance accommodation and Q_s, most of the accommodation was generated during the pulse. As a result, this period had an excess of accommodation generation relative to Q_s, which drove the transgression. Based on observations of channel mobility and shoreline position, complete recovery after the tectonic pulse took approximately 16 hr (Fig. 11C–F).

Measuring Surface Reworking Time.—Similarly to the steady-deformation stages, we measure the average wet percent of the delta top over

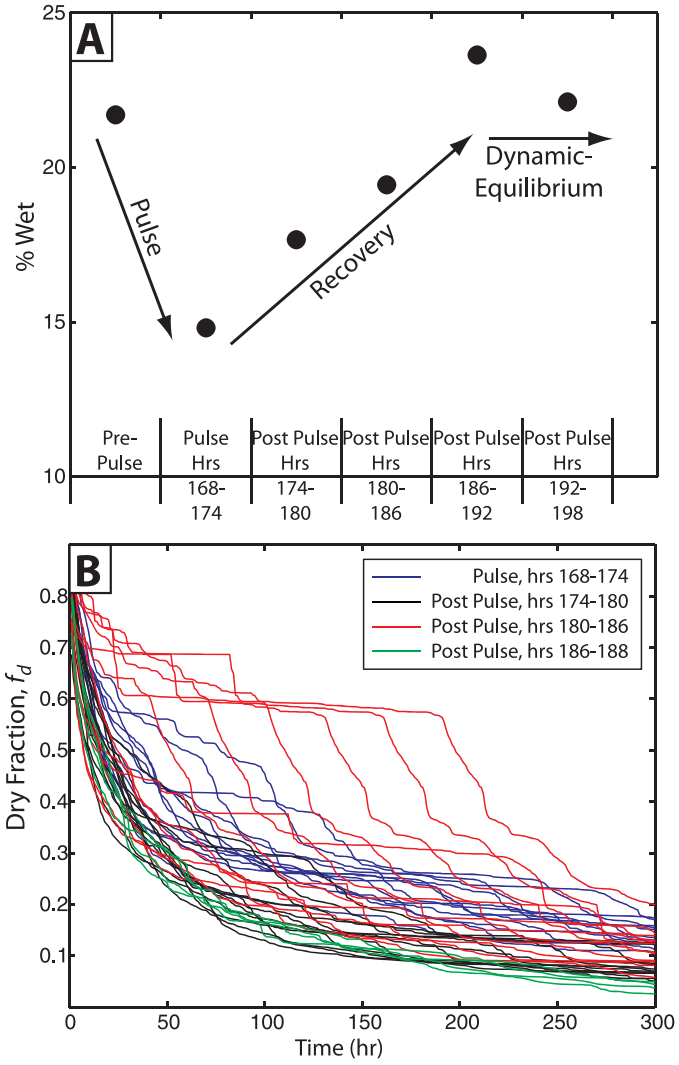

FIG. 12.—defining the lateral extent and mobility of channels in the pulse–interpulse cycle of XES 08 stage 1. **A)** Average percent of the delta top occupied by channels measured every six hours of the pulse–interpulse cycle. **B)** 48 dry-fraction reduction curves characterizing the mobility of channels in the pulse–interpulse cycle. Curves initiated every 0.5 hours of stage 4, each including every 1 min measurement of channel locations. Curves are colored by relative time in the pulse–interpulse cycle.

the course of the pulse–interpulse cycle and monitor the dry fraction reduction through time. During the 16 hour interpulse period that preceded the pulse, the average fraction of the delta top covered by flow was 22%. This value rapidly reduced to 15% during the six hours of pulse activity, followed by a gradual increase during the first 12 hours post-pulse until the average percentage of the delta top covered by flow approached its pre-pulse value, at which point it remained for the final 12 hours of the experiment (Fig. 12A).

Only a minor increase in t_{95} was observed during the pulse (Fig. 4B, 12B), which was followed by $>$ 6 hr of low t_{95}, (thus rapid f_d reduction). During hours 180–186, as flow was pinned over the inboard region of uplift and subsidence maximum, we observed a second peak in t_{95} (thus slow reduction in f_d). However, the magnitudes of the two dominant peaks during the pulse–interpulse cycle were much less than the peak in t_{95} observed during the steady-deformation Stage 3, which had the same Q_s and Q_w as well as similar T_* to the pulsed Stage 4. The final 12 hours of Stage 4 had low t_{95}. The average t_{95} of Stage 4 was 13.2 h, far less than the steady XES 08 Stage 3, which had an average $t_{95} = 21.5$ h (Fig. 5D).

Steering though Preferential Flow Occupation.—We generate flow-occupation maps for six-hour time windows that cover the period of pulsed tectonics and the interpulse period that followed (Fig. 13A, C, E, G, I). We compare these to isopach maps over the same time windows generated through differencing of topographic maps corrected for basin subsidence (Fig. 13B, D, F, H, J) in a manner analogous to Martin et al. (2009). During the six hours of the pulse we see no zones of enhanced flow occupation that are spatially correlated with subsidence trends, but during this period significant deposition occurred in the relay zone as accommodation was created and significant erosion occurred in the area of uplift above the inboard fault. These trends, for the most part, continued for the first six hours after the pulse. Between 6 and 12 hr, post-pulse flow occupation maps reveal a path of most frequent descent over the inboard zone of uplift and into the subsidence maximum. During this time more sedimentation occurred in the subsidence maximum than in any other six hour window. Interestingly, the inboard zone of uplift during the pulse was characterized by a mixture of erosion and deposition. During the remaining 12 hours of the experiment, the zone of maximum subsidence was only slightly enhanced in flow occupation relative to other regions and deposition was relatively homogeneous over the entire delta top.

Finally, we compared the flow-occupation map for XES 08 Stage 3 to a flow-occupation map generated for the full pulse–interpulse cycle in Stage 4. We observe a similar trend in flow occupation between the two stages, with the path of most frequent descent migrating over the inboard zone of uplift and into the subsidence maximum. However, the magnitude of this trend in the full pulse–interpulse cycle of stage 4 is muted in comparison to XES 08 Stage 3 (Fig. 14).

Stratigraphy

Deposits of Stage 4 are identified in images of the preserved stratigraphy as having a slight orange tint. The first observation is a transgression, then progradation, of the sand–coal boundary at the bottom of the Stage 4 deposits (Figs. 9, 10). This transgression is similar to those observed at earlier stage boundaries in XES 08 and within the XES 05 Stage 1 deposit. We note, though, that Q_s and Q_w were kept constant for 68 hr prior to deposition of sediment occurring during the observed transgression.

Our second major observation deals with the geometry of stratal boundaries resulting from the pulse–interpulse period. The imbalance of Q_s relative to accommodation during the pulse resulted in generation of unfilled accommodation that was filled in the following interpulse period when Q_s exceeded the rate of accommodation. Much of this space was filled by sediment eroded from the inboard region of uplift and deposited from flow expansion in the subsidence maximum as lobate deposits. This process resulted in progradation of a subaerially deposited sediment wedge in the relay zone which downlapped onto the depositional surface present at the end of the pulse (Fig. 15A, B). This geometry is in contrast to the roughly parallel stratal boundaries present in most of the steady-deformation stratigraphy or the topset–forset–bottomset packages resulting from delta progradation into autogenic lakes during XES 05 Stage 1 (Fig. 15C, D).

Third, we observe a large cluster of channel bodies in the stage 4 stratigraphy near the tip of the inboard fault (the region where lateral subsidence gradient is maximized) constructed of channel scours that range from 10 to 20 mm in thickness (Fig. 16). It is difficult to statistically characterize changes in channel-body stacking that occur near the fault tips between stages, due to the limited thickness of preserved strata. However, we note that the channel-body cluster near the tip of the inboard fault, which measures more than 0.15 m in width and $\sim$ 0.04 m

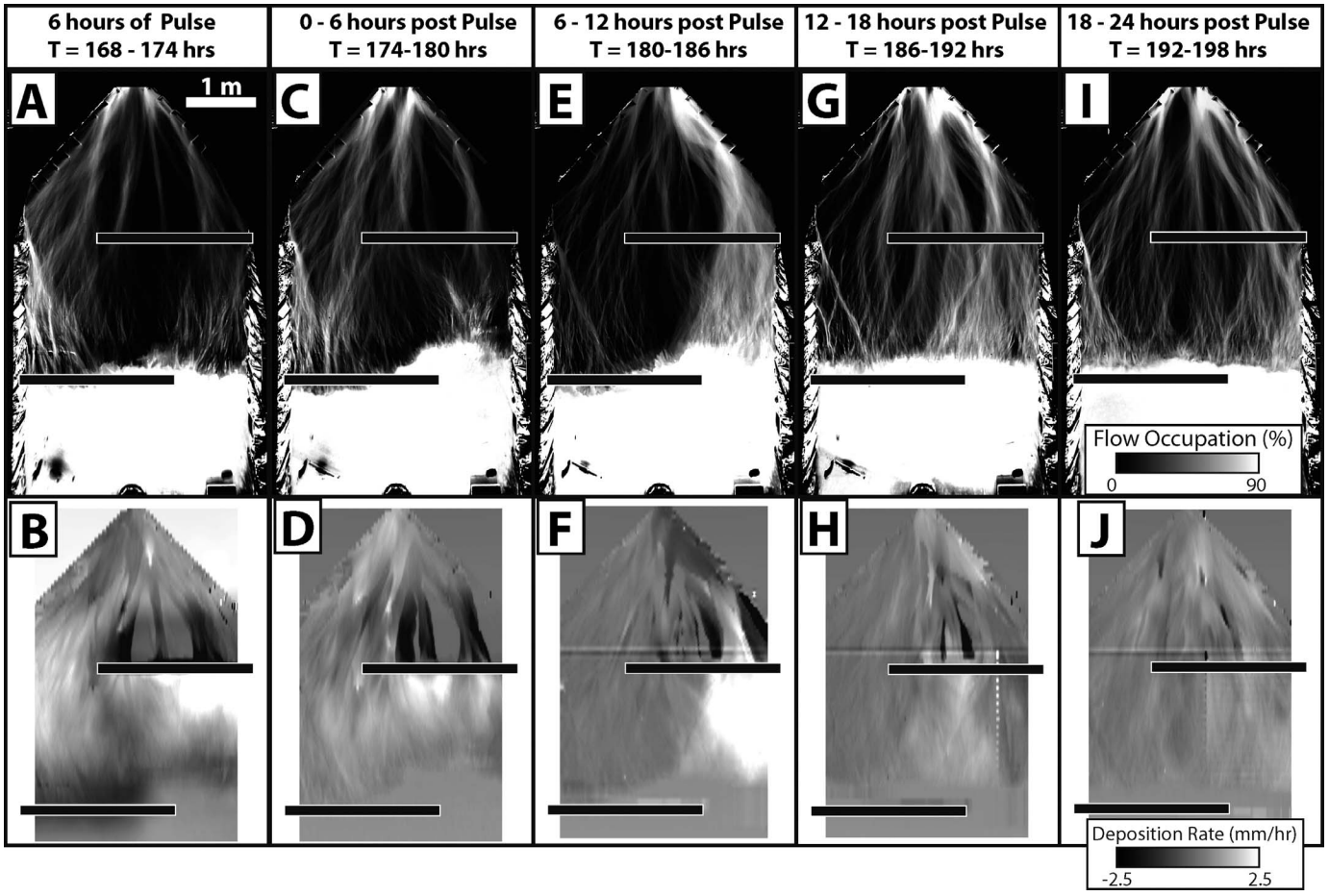

FIG. 13.—Time-integrated flow-occupation maps and sedimentation-rate maps spanning every six hours of run time for complete pulse–interpulse cycle of XES 08 stage 4. For flow-occupation maps, white denotes continuous occupation over the full experimental stage, whereas black denotes no flow occupation. For sedimentation-rate maps, aggradation increases as color becomes brighter. Location of inboard and outboard faults are shown by black rectangles.

in thickness, is larger than any other channel-body cluster we observe in stages 3 or 4 and that it occurs over the relay zone.

Interpretation

The tectonic pulses were designed with an estimated $S_x = 0.049$, equal to S_x of XES 05 stage 1. As discussed previously, while Q_s/Q_w was held constant between the two stages, S_x of XES 08 stage 4 was slightly greater than during XES 05 stage 1, resulting in an increase of $T_{t,pulse}$ relative to our initial prediction. As such $T_{t,pulse}$ was slightly greater than the duration of the pulse, $\frac{T_{t,pulse}}{T_p} = 1.2$. Further, due to settling of the wooden wall, used to define the inboard fault, on the subsidence cells at the base of the XES basin, we were able to run only one pulse–interpulse cycle.

Comparison of surface flow in XES 08 stage 3 and 4 reveals that the addition of a tectonic pulse characterized by three times the background tectonic rates of XES 08 stage 3, but with $\frac{T_{t,pulse}}{T_p} > 1$, was not sufficient to promote enhanced flow occupation over the subsidence maximum. This is in agreement with the initial hypothesis presented above on the combination of strength and length necessary for a pulse to cause steering of channels. However, given our experimental parameters we cannot characterize the morphodynamics associated with a pulse, including the strength of resulting steering and the time to regrade a system following a pulsed coseismic event with $\frac{T_{t,pulse}}{T_p} < 1$.

DISCUSSION

Steering Associated with Steady Subsidence

Observations of channel and channel-body orientation from three field locations lend support to the utility in using T_* to estimate the degree of channel steering. Kim et al. (2010) used field data gathered by Leeder et al. (1996) for the Rio Grande rift, New Mexico, and by Peakall (1998) for the Carson River, Nevada, to characterize the two systems as tectonic-dominated with T_* values in excess of unity. These estimates are in good agreement with field observations from the two systems that suggest that channels have been steered into regions of high subsidence.

In contrast to the two field systems discussed above, a recent study by Armstrong et al. (in press) investigate channel interactions with growth faults on the Mississippi Delta top. The Mississippi Delta hosts a large number of active growth faults that have been identified in southeastern Louisiana from surface geomorphology and subsurface data (Gagliano et al. 2003). These faults are associated with movement of the Louann Salt in response to loading through the Quaternary (Salvador 1991). A survey of fault characteristics in this region by George (2008) found typical fault widths on the order of 10 km with lateral subsidence-rate gradients on the order of 1×10^{-9} yr^{-1}. Fault associated subsidence is maximized near fault midpoints and tapers to near-zero values at fault tips. In this region, S_x can be approximated as 1.4×10^{-5} m/m. These parameters result in a $T_t = 14{,}000$ yr. Estimation of T_c is more difficult given temporal variability in channel

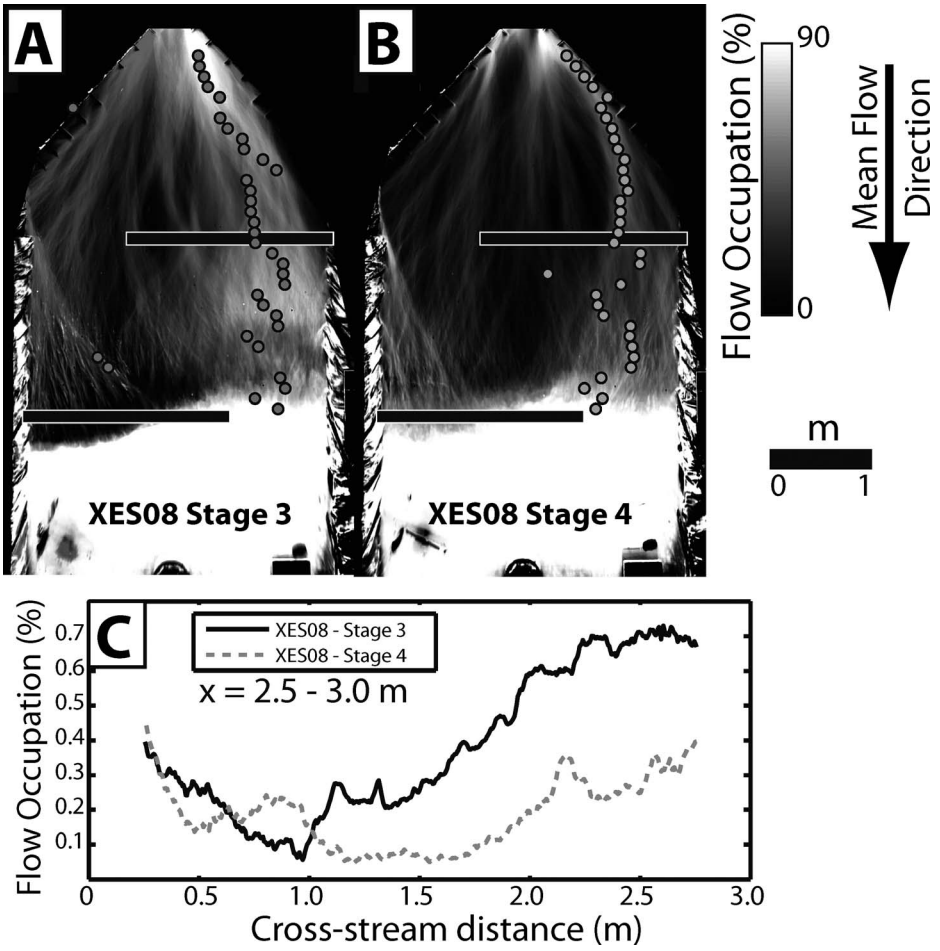

FIG. 14.—Comparison of XES 08 stages 3 and 4. Two stages share similar long-term T_* values, with aseismic subsidence in stage 3 and coseismic subsidence in stage 4. **A**, **B)** Time-integrated flow-occupation maps for stage 3 and pulse–interpulse cycle of stage 4. White denotes continuous occupation over the full experimental stage, whereas black denotes no flow occupation. White circles denote cross-stream maximum in flow occupation for cross-stream sections sharing constant x distance from source, spatially averaged at 0.1 m increments in the x direction. Location of inboard and outboard faults are shown by black rectangles. **C)** Time-integrated flow occupation in the relay-ramp zone.

characteristics, river valley width, and sediment load. Using mapping of Mississippi Delta lobe locations and associated deposit dates from Fisk (1954), we estimate that points on the Mississippi Delta top are on average revisited by surface flow every 5,000–10,000 yr. We use this number as our T_c estimate, yielding a T_* of 0.36–0.71. Subsurface mapping in the vicinity of the growth faults shows no noticeable channel steering for 90% of 70 channel bodies (Armstrong et al. in press). Thus, similarly to our experiments, it appears T_* values in excess of 0.6–0.7 are necessary to result in significant steering of channels via lateral subsidence gradients.

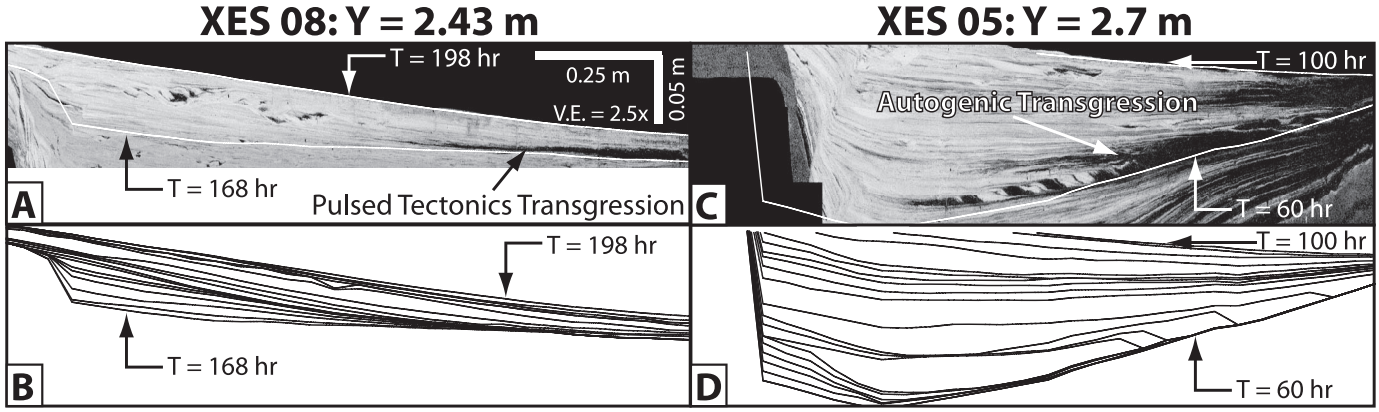

FIG. 15.—Dip sections of experimental deposit sliced in the downstream direction in the zone of maximum subsidence of XES 05 and 08 and their associated reconstructed strata geometry from surface scans. Cross sections are presented to highlight observed facies transgression associated with pulsed tectonics of XES 08 stage 4 and autogenic lake formation during XES 05 stage 1.

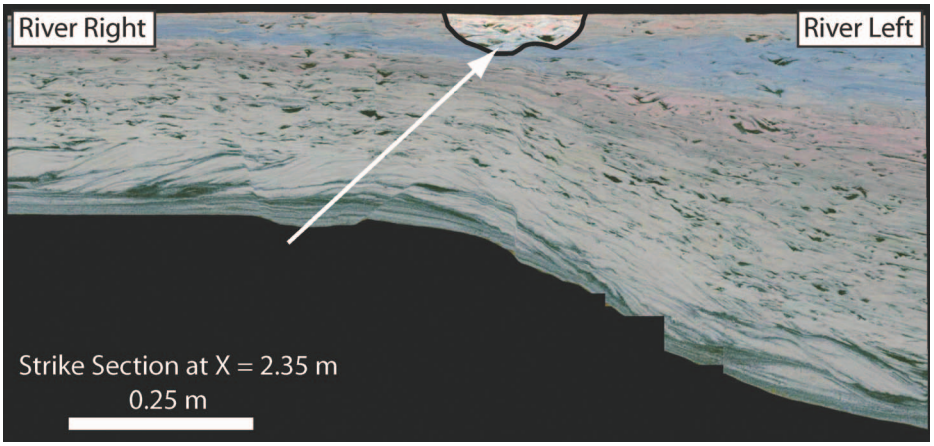

FIG. 16.—Strike section of XES 08 experimental deposit sliced in the cross-stream direction at $x = 2.35$ m. This cross section is located immediately downstream of the inboard fault. Channel-body cluster in stage 4 is highlighted.

Steering Associated with Pulsed Subsidence

While we did not find significant channel steering associated with pulsed subsidence in our experiments, evidence for this style of steering is seen in field-scale systems. A recent study of the Brahmaputra River in the upper Assam valley of India detailed the response of the system to a magnitude 8.0 earthquake in 1950 (Lahiri and Sinha 2012). Lahiri and Sinha detail a rapid migration of the Brahmaputra River into regions of high lateral subsidence in the river valley following the 1950 Assam earthquake. Using given and estimated parameters based on data in Lahiri and Sinha (2012) and Islam et al. (1999) we have: $B_t = 4.5 \times 10^4$ m, $B_w = 1.0 \times 10^4$ m, $q_s/h = 7.94 \times 10^2$ m/yr, $S_x = 2.5 \times 10^{-4}$ m/m, and $\Delta\sigma/L_y = 2.4 \times 10^{-9}$ yr^{-1}. These values yield a T_* estimate of 4×10^{-4}, thus extremely channel dominated. This result is possibly unsurprising given the high sediment discharge rates of the Brahmaputra River and the small valley width in this region. These estimates of the long-term T_* of this system support the interpretation by Lahiri and Sinha (2012) that the observed channel steering is associated with the 1950 earthquake and not the longer-term subsidence rates.

Allogenic and Autogenic Facies Transgressions in Relay-Ramp Stratigraphy

Strata preserved in our two experiments contain facies transitions associated with both allogenic forcings and autogenic processes. Starting with the allogenic forcings, we observe a rapid transgression followed by progradation of the sand–coal boundary preserved in the strata deposited at the start of XES 08 stages 2 and 3. These retrogradational strata were associated with reductions in both Q_s and Q_w across the stage boundaries. While the ratio of Q_s/Q_w was kept constant, the reduction of these individual components forced a temporary increase in proximal deposition while the deposit surface regraded to a higher equilibrium slope. The pulsed-tectonics stage also resulted in allogenic retrogradation followed by progradation of the sand–coal boundary. This resulted from temporal changes in the ratio of input Q_s to generation of accommodation during this stage. During the pulsed subsidence, accommodation generation outpaced sediment delivery to the basin and led to the temporary retrogradation. In contrast to the allogenic retrogradation discussed above, two phases of retrogradation of the sand–coal boundary are visible in the stratigraphy of the aseismic XES 05 stage 1. As detailed in Kim et al. (2010) this stratigraphic packaging was created during long-period autogenic sedimentation cycles during the tectonically dominated stage. The strong tectonics relative to channel mobility in this stage resulted in the formation of a lake in the subsidence maximum as sediment was deposited by flow that was temporarily steered towards the river-right side of the basin. Progradation of the coal–sand boundary then occurred as deltas, fed from eroded sediment sourced from the inboard region of uplift, filled the autogenic lakes. The similar stratigraphic signatures of the autogenic facies transgression and the two types of allogenic facies transgressions highlights the difficulty in definitively distinguishing among them in the stratigraphic record.

CONCLUSIONS

Our experiments support previous suggestions that the ability of lateral basin tilting to steer channels towards subsidence maxima is set by lateral gradients in subsidence rates relative to lateral mobility of channels. In settings where the lateral mobility of channels is high relative to lateral subsidence-rate gradients (XES 08 Stage 1), little steering occurs as channels are able to rework surface topography rapidly enough that topographic lows associated with the tectonic regime do not develop. In settings where the lateral mobility of channels is low relative to lateral subsidence rate gradients (XES 05 Stage 1), strong steering occurs as topographic lows associated with the tectonic field can develop prior to being filled by the transport system.

Stages characterized by strong tectonic subsidence relative to channel mobility in our experimental relay-ramp setting influenced surface dynamics in the following ways: flow deflection into the subsidence maximum; preference for channel occupation over both the subsidence maximum and the inboard zone of uplift; and reduction of channel mobility relative to settings with the same water and sediment input but spatially uniform subsidence.

The ability of lateral gradients to steer channels depends on the sign of the relative surface motion: lateral gradients in subsidence alone result in a preference for occupation over the subsidence maximum and enhanced channel stacking density in resulting stratigraphy. Further, gradients that include uplift result in a preference for flow occupation in the zone of uplift. This occurs due to formation of incised, low-mobility channels over the zone of relative uplift.

Retrogradation and progradation of the quartz–coal boundary in the deposit stratigraphy, associated with variable subsidence, can be linked to both allogenic forcing and autogenic surface processes. Allogenic forcing includes changes in input water and sediment supplies and temporally variable subsidence rates. Autogenic processes associated with transgressions include the development of marine autogenic depressions over subsidence maxima due to tectonically driven reduction of channel mobility.

Theory to predict when pulsed subsidence in alluvial basin results in channel steering suggests that pulsed subsidence must be associated with high lateral gradients in subsidence rate over a duration long enough to generate cross-basin surface slope comparable to the regional down-basin surface slope. An experimental stage designed to test this hypothesis is consistent with the theory.

ACKNOWLEDGMENTS

We thank Dick Christopher, Jim Mullin, and Chris Ellis for help designing and conducting experiments discussed in this manuscript. Further we thank David Mohrig for fruitful discussions that aided the crafting of this manuscript. We wish to thank our associate editor Peter Burgess and an anonymous reviewer for constructive reviews. Support for our research was provided by the St. Anthony Falls Laboratory Industrial Consortium (BHP Billiton, Chevron, ConocoPhilips, ExxonMobil, Japan National Oil Company, and Shell) and by the Science and Technology Center Program of the National Science Foundation via the National Center for Earth-Surface Dynamics under agreement EAR-0120914. Additionally we thank Penny Patterson (ExxonMobil) and Sanjeev Gupta (Imperial College London) for advice in designing the experiment. A link to the supplemental movie is available from JSR's Data Archive: http://sepm.org/pages.aspx?pageid=229.

REFERENCES

Alexandar, J., and Leeder, M.R., 1987, Active tectonic control of alluvial architecture, *in* Ethridge, F.G., Flores, R.M., and Harvey, M.D., eds., Recent Developments in Fluivial Sedimentology: SEPM, Special Publication 39, p. 243–252.

Alexander, J., and Leeder, M.R., 1990, Geomorphology and surface tilting in an active extensional basin, SW Montana, USA: Geological Society of London, Journal, v. 147, p. 461–467.

Allen, J.R.L., 1978, Studies in fluviatile sedimentation: an exploratory quantitative model for the architecture of avulsion-controlled alluvial sites: Sedimentary Geology, v. 26, p. 617–644.

Allen, P.A., and Densmore, A.L., 2000, Sediment flux from an uplifting fault block: Basin Research, v. 12, p. 367–380.

Armstrong, C., Mohrig, D., Hess, T., George, T., and Straub, K.M., in press, Influence of growth faults on coastal fluvial systems: examples from the late Miocene to Recent Mississippi River Delta: Sedimentary Geology.

Bridge, J.S., and Leeder, M.R., 1979, A simulation model of alluvial stratigraphy: Sedimentology, v. 26, p. 617–644.

Cazanacli, D., Paola, C., and Parker, G., 2002, Experimental steep, braided flow: application to flooding risk on fans: Journal of Hydraulic Engineering, v. 128, p. 322–330.

Cowie, P.A., and Shipton, Z.K., 1998, Fault tip displacement gradients and process zone dimensions: Journal of Structural Geology, v. 20, p. 983–997.

Densmore, A.L., Dawers, N.H., Gupta, S., Allen, P.A., and Gilpin, R., 2003, Landscape evolution at extensional relay zones: Journal of Geophysical Research, Solid Earth, v. 108, doi: 10.1029/2001JB001741.

Dorsey, R.J., and Umhoefer, P.J., 2000, Tectonic and eustatic controls on sequence stratigraphy of the Pliocene Loreto basin, Baja California Sur, Mexico: Geological Society of America, Bulletin, v. 112, p. 177–199.

Ellis, M.A., Densmore, A.L., and Anderson, R.S., 1999, Development of mountainous topography in the Basin Ranges, USA: Basin Research, v. 11, p. 21–41.

Fisk, N.H., 1954, Late Quaternary deltaic deposits of the Mississippi River, Geological Society of America, Special Papers, v. 62, p. 279–302.

Gagliano, M.S., Burton Kemp, E.I., Wicker, K.M., Wiltenmuth, K.S., and Sabate, R.W., 2003, Neo-tectonic framework of Southeast Louisiana and applications to coastal restoration: Gulf Coast Assiciation of Geological Societies and SEPM, Gulf Coast Section, Transactions, v. 53, p. 262–276.

George, T.J., 2008, 3D seismic evaluation of fault control on Quaternary subsidence patterns, rates, and related surface morphology in Southeastern Louisiana [Master's thesis]: Austin, University of Texas at Austin.

Gouw, M.J.P., 2008, Alluvial architecture of the Holocene Rhine–Meuse delta (the Netherlands): Sedimentology, v. 55, p. 1487–1516.

Gupta, S., Underhill, J.R., Sharp, I.R., and Gawthorpe, R.L., 1999, Role of fault interactions in controlling synrift sediment dispersal patterns: Miocene, Abu Alaqa Group, Suez Rift, Sinai, Egypt: Basin Research, v. 11, p. 167–189.

Heller, P.L., Paola, C., Hwang, I., John, B., and Steel, R., 2001, Geomorphology and sequence stratigraphy due to slow and rapid base-level changes in an experimental subsiding basin (XES 96-1): American Association of Petroleum Geologists, Bulletin, v. 85, p. 817–838.

Hickson, T.A., Sheets, B.A., Paola, C., and Kelberer, M., 2005, Experimental test of tectonic controls on three-dimensional alluvial facies architecture: Journal of Sedimentary Research, v. 75, p. 710–722.

Humphrey, N.F., and Konrad, S.K., 2000, River incision or diversion in response to bedrock uplift: Geology, v. 28, p. 43–46.

Islam, M.R., Begum, S.F., Yamaguchi, Y., and Ogawa, K., 1999, The Ganges and Brahmaputra rivers in Bangladesh: basin denudation and sedimentation: Hydrological Processes, v. 13, p. 2907–2923.

Kim, W., and Paola, C., 2007, Long-period cyclic sedimentation with constant tectonic forcing in an experimental relay ramp: Geology, v. 35, p. 331–334.

Kim, W., Sheets, B., and Paola, C., 2010, Steering of experimental channels by lateral basin tilting: Basin Research, v. 22, p. 286–301.

Kim, W., Connell, S.D., Steel, E., Smith, G.A., and Paola, C., 2011, Mass-balance control on the interaction of axial and transverse channel systems: Geology, v. 39, p. 611–614.

Kraus, M.J., 1992, Alluvial response to differential subsidence: sedimentological analysis aided by remote-sensing, Willwood Formation (Eocene), Bighorn Basin, Wyoming, USA: Sedimentology, v. 39, p. 455–470.

Lahiri, S.K., and Sinha, R., 2012, Tectonic controls on the morphodynamics of the Brahmaputra River system in the upper Assam valley, India: Geomorphology, v. 169–170, p. 74–85.

Larsen, P.H., 1988, Relay structures in a Lower Permian basement-involved extension system, East Greenland: Journal of Structural Geology, v. 10, p. 3–8.

Leeder, M.R., 1978, A quantitative stratigraphic model for alluvium, with special reference to channel deposit density and interconnectedness, *in* Miall, A.D., ed., Fluvial Sedimentology: Canadian Society of Petroleum Geologists, Memoir 5, p. 587–596.

Leeder, M.R., Mack, G.H., Peakall, J., and Salyards, S.L., 1996, First quantitative test of alluvial stratigraphic models: Southern Rio Grande rift, New Mexico: Geology, v. 24, p. 87–90.

MacCarthy, I.A.J., 1990, Alluvial sedimentation patterns in the Munster Basin, Ireland: Sedimentology, v. 37, p. 685–712.

Mack, G.H., and Seager, W.R., 1990, Tectonic control on facies distribution of the Camp Rice and Palomas formations (Pliocene–Pleistocene) in the Southern Rio-Grande Rift: Geological Society of America, Bulletin, v. 102, p. 45–53.

Mackey, S.D., and Bridge, J.S., 1995, 3-dimensional model of alluvial stratigraphy: theory and application: Journal of Sedimentary Research, v. 65, p. 7–31.

Mackin, J.H., 1948, Concept of the graded river: Geological Society of America, Bulletin, v. 59, p. 463–512.

Martin, J., Paola, C., Abreu, V., Neal, J., and Sheets, B., 2009, Sequence stratigraphy of experimental strata under known conditions of differential subsidence and variable base level: American Association of Petroleum Geologists, Bulletin, v. 93, p. 503–533.

Marzo, M., Nijman, W., and Puigdefabregas, C., 1988, Architecture of the Castissent fluvial sheet sandstones, Eocene, south Pyrenees, Spain: Sedimentology, v. 35, p. 719–738.

Melvin, J., 1993, Evolving fluvial style in the Kekiktuk Formation (Mississippian), Endicott Field area, Alaska: base-level response to contemporaneous tectonism: American Association of Petroleum Geologists, Bulletin, v. 77, p. 1723–1744.

Mullin, J., and Ellis, C., 2008, Method to produce grain-scale digital images of large experimental sedimentary deposits and other imperfectly flat stratigraphy: Journal of Sedimentary Research, v. 78, p. 239–244.

Ouchi, S., 1985, Response of alluvial rivers to slow active tectonic movement: Geological Society of America, Bulletin, v. 96, p. 504–515.

Paola, C., 2000, Quantitative models of sedimentary basin filling: Sedimentology, v. 47, p. 121–178.

Paola, C., and Borgman, L., 1991, Reconstructing random topography from preserved stratification: Sedimentology, v. 38, p. 553–565.

Paola, C., Heller, P.L., and Angevine, C.L., 1992, The large-scale dynamics of grain-size variation in alluvial basins, 1: Theory: Basin Research, v. 4, p. 73–90.

Paola, C., Mullin, J., Ellis, C., Mohrig, D., Swenson, J.B., Parker, G., Hickson, T., Heller, P.L., Pratson, L., Syvitski, J.P.M., Sheets, B., and Strong, N., 2001, Experimental Stratigraphy: GSA Today, v. 1, p. 4–9.

Parker, G., Paola, C., Whipple, K.X., and Mohrig, D., 1998a, Alluvial fans formed by channelized fluvial and sheet flow. I: Theory: Journal of Hydraulic Engineering, v. 124, p. 985–995.

Parker, G., Paola, C., Whipple, K.X., Mohrig, D., Toro-Escobar, C.M., Halverson, M., and Skoglund, T.W., 1998b, Alluvial fans formed by channelized fluvial and sheet flow. II: Application: Journal of Hydraulic Engineering, v. 24, p. 996–1004.

Peakall, J., 1998, Axial river evolution in response to half-graben faulting: Carson River, Nevada, USA: Journal of Sedimentary Research, v. 68, p. 788–799.

Peakall, J., Leeder, M., Best, J., and Ashworth, P., 2000, River response to lateral ground tilting: a synthesis and some implications for the modelling of alluvial architecture in extensional basins: Basin Research, v. 12, p. 413–424.

Price, S.P., and Scott, B., 1991, Pliocene Burdur Basin, SW Turkey: tectonics, seismicity and sedimentation: Geological Society of London, Journal, v. 148, p. 345–354.

Ryseth, A., and Ramm, M., 1996, Alluvial architecture and differential subsidence in the Statfjord Formation, North Sea: prediction of reservoir potential: Petroleum Geoscience, v. 2, p. 271–287.

Salvador, A., 1991, Origin and development of the Gulf of Mexico Basin, *in* Salvador, A., ed., The Gulf of Mexico Basin: Geological Society of America, The Geology of North America, v. J, p. 131–180.

Schumm, S.A., Mosley, M.P., and Weaver, W.E., 1987, Experimental Fluvial Geomorphology: New York, USA, John Wiley & Sons, 301 p.

Sheets, B., 2004, Assembling the Alluvial Stratigraphic Record: Spatial and Temporal Sedimentation Patterns in Experimental Alluvial Systems [Ph.D. thesis]: Minneapolis, Minnesota, University of Minnesota.

Sheets, B.A., Hickson, T.A., and Paola, C., 2002, Assembling the stratigraphic record: depositional patterns and time-scales in an experimental alluvial basin: Basin Research, v. 14, p. 287–301.

Shen, Z., Tornqvist, T.E., Autin, W.J., Mateo, Z.R.P., Straub, K.M., and Mauz, B., 2012, Rapid and widespread response of the Lower Mississippi River to eustatic forcing during the last glacial–interglacial cycle: Geological Society of America, Bulletin, v. 124, p. 690–704.

Snow, R.S., and Slingerland, R.L., 1990, Stream profile adjustment to crustal warping: nonlinear results from a simple-model: Journal of Geology, v. 98, p. 699–708.

Strong, N., Sheets, B.A., Hickson, T.A., and Paola, C., 2005, A mass-balance framework for quantifying downstream changes in fluvial architecture, *in* Blum, M., Marriott, S., and Leclair, S., eds., Fluvial sedimentology VII: International Association of Sedimentologists, Special Publication 35, p. 243–253.

Wells, D.L., and Coppersmith, K.J., 1994, New empirical relationships among magnitude, rupture length, rupture width, rupture area, and surface displacement: Seismological Society of America, Bulletin, v. 84, p. 974–1002.

Whipple, K.X., Parker, G., Paola, C., and Mohrig, D., 1998, Channel dynamics, sediment transport, and the slope of alluvial fans: experimental study: Journal of Geology, v. 106, p. 677–693.

Wickert, A.D., Martin, J.M., Tal, M., Kim, W., Sheets, B., and Paola, C., 2013, River channel lateral mobility: metrics, time scales, and controls: Journal of Geophysical Research Earth Surface, v. 118, p. DOI: 10.1029/2012JF002386.

Received 22 January 2013; accepted 3 October 2013.